Lithos 258–259 (2016) 149–162

Contents lists available at ScienceDirect

Lithos

journal homepage: www.elsevier.com/locate/lithos

Petrogenesis and geodynamic setting of Early Cretaceous mafic–ultramafic intrusions, South China: A case study from the Gan–Hang tectonic belt

Youqiang Qi [a,e,*], Ruizhong Hu [a,**], Shen Liu [b], Ian M. Coulson [c], Huawen Qi [a], Jianji Tian [d], Jingjing Zhu [a]

[a] State Key Laboratory of Ore Deposit Geochemistry, Institute of Geochemistry, Chinese Academy of Sciences, Guiyang 550081, PR China
[b] State Key Laboratory of Continental Dynamics and Department of Geology, Northwest University, Xi'an 710069, PR China
[c] Solid Earth Studies Laboratory, Department of Geology, University of Regina, Regina, Saskatchewan S4S 0A2, Canada
[d] Beijing Research Institute of Uranium Geology, Beijing 100029, PR China
[e] EGRU (Economic Geology Research Centre), College of Science, Technology and Engineering, James Cook University, Townsville, Queensland 4811, Australia

ARTICLE INFO

Article history:
Received 28 October 2015
Accepted 23 April 2016
Available online 4 May 2016

Keywords:
Mafic–ultramafic intrusions
Petrogenesis
Pyroxenite
Subcontinental lithospheric mantle (SCLM)
Early Cretaceous
Gan–Hang Tectonic Belt (GHTB)

ABSTRACT

A study using whole-rock major-trace elements and Sr–Nd isotopes as well as zircon U–Pb dating has been carried out on Early Cretaceous mafic–ultramafic intrusions from the Gan–Hang tectonic belt (GHTB), South China, to understand the origin of mantle sources and the sequential evolution of the underlying Late Mesozoic lithospheric mantle of this area. The study focused on two intrusions, one at Quzhou and the other at Longyou (see Fig. 1). They are primarily composed of mafic–ultramafic rocks with wide range of chemical compositions. The Quzhou mafic rocks have relatively narrow ranges of SiO_2 (48.94–51.79 wt%), MgO (6.07–7.21 wt%), Fe_2O_3 (10.48–11.56 wt%), CaO (8.20–8.81 wt%), and $Mg^{\#}$ (51.7–56.5) with relatively low K_2O (0.56–0.67 wt%) and Na_2O (3.09–3.42 wt%). By contrast, the ultramafic rocks from Longyou have distinct lower SiO_2 (41.50–45.11 wt%) and higher MgO (9.05–9.90 wt%), Fe_2O_3 (12.14–12.62 wt%), CaO (8.64–10.67 wt%), and $Mg^{\#}$ (59.5–61.1) with relatively higher K_2O (1.32–1.75 wt%) and Na_2O (4.53–5.08 wt%). They are characterized by Ocean Island Basalts (OIB)-type trace element distribution patterns, with a significant enrichment of light rare earth elements (LREE), large ion lithophile elements (LILE, i.e., Rb, Ba, K, and Sr) and high field strength elements (HFSE, i.e., Nb, Ta), and slight depletion of Th, U, Ti, and Y. The intrusions exhibit relatively depleted Sr–Nd isotope compositions, with $(^{87}Sr/^{86}Sr)_i$ range of 0.7035 to 0.7055 $(^{143}Nd/^{144}Nd)_i$ of 0.51264 to 0.51281 and $\varepsilon_{Nd}(t)$ values of +3.0 to +6.6. Zircon U–Pb dating of Longyou and Quzhou intrusions yields consistent magma emplacement ages of 129.0 ± 3.9 to 126.2 ± 2.4 Ma, respectively. The dating results are consistent with the peak of extension in Early Cretacerous throughout the Gan–Hang tectonic belt. Their magmas were principally derived from near-solidus partial melting of pyroxenites with different content of silica, and the pyroxenites were resulted from a juvenile SCLM peridotite metasomatized by adakitic and felsic melts under a subducted oceanic crust-lithospheric mantle in Neoproterozoic. During the subduction of the oceanic crust, the juvenile SCLM can be sandwiched by the ancient SCLM above and the pyroxenites below and stored for hundreds of millions of years until Late Mesozoic. Then partial melting of the pyroxenites was triggered during the peak of extension in response to the tectonic reactivation of the GHTB in Early Cretaceous. It is clear that fault reactivation and structural constraints within the GHTB had played an important role in its magmatic evolution.

1. Introduction

Multiple episodes of Mesozoic magmatism in the South China Block (SCB) have produced widespread igneous rocks, including broadly bimodal suites of tholeiitic basalt–rhyolite volcanic rocks and minor mafic–ultramafic intrusions and extensive swarms of mafic dykes. This igneous episode is associated with large-scale extensional tectonics through much of South China. The tectonic regime responsible for Mesozoic magmatism in South China has been an issue of debate, mainly focusing on the timing of events and the detailed mechanisms involved (e.g., Chen et al., 2005, Hu et al., 2004, 2008, Hua et al., 2005, Li and Li, 2007, Li et al., 2007, Mao et al., 2004, 2007, 2008, Wang, 2004, Wang et al., 2003, 2005, 2006, Xu, 2008, Zhou, 2003). Current views on the evolution of the Mesozoic lithosphere across Southern China are dominated by two schools of thought. The first invokes a subduction regime, although the details of individual models vary, including an Andean-

* Correspondence to: State Key Laboratory of Ore Deposit Geochemistry, Institute of Geochemistry, Chinese Academy of Sciences, Guiyang, 550081, PR China. Tel.: +86 851 5891962; fax: +86 851 5891664.
** Corresponding author. Tel.: +86 851 5891962; fax: +86 851 5891664.
E-mail addresses: qiyouqiang@sina.com (Y. Qi), huruizhong@vip.gyig.ac.cn (R. Hu).

http://dx.doi.org/10.1016/j.lithos.2016.04.027

type active continental margin (Charvet et al., 1994), subduction of the Pacific Plate with associated underplating of basaltic magma (Zhou and Li, 2000), and a low angle of subduction for the down-going Pacific slab (Li and Li, 2007; Zhu et al., 2010). The second school believes that the magmatism was caused by intracontinental lithospheric extension and thinning, which was accompanied by asthenospheric upwelling (Chen and Jahn, 1998; Fan et al., 2003; Gilder et al., 1996; Li et al., 2003, 2004; Wang et al., 2003, 2004a, 2004b, 2005).

Previous studies have suggested that the Archaean and Proterozoic mantle that once existed beneath the SCB has been largely or completely removed and replaced by younger, hotter, and more fertile mantle (Xu et al., 2000, 2002). However, it remains unclear when the mantle thinning and replacement processes occurred. In contrast to the widespread distribution of Cenozoic basalts, Mesozoic basaltic rocks only sporadically occur inland of the SCB (Jiang et al., 2009; Li et al., 2004; Wang et al., 2003, 2004a, 2004b, 2005; Xie et al., 2005a; Xu and Xie, 2005; Zhao et al., 1998). Hence, Mesozoic mantle-derived rocks, especially the Mesozoic mafic–ultramafic intrusions, can provide constraints on the different controversial models pertaining to the evolution of lithosphere beneath the SCB.

In addition, deep-shear faults can undermine the integrity of the lithosphere and consequently trigger a series of tectono-chemical processes with a result of transforming the nature of the lithospheric mantle, but only a few studies have addressed this issue (Wu et al., 2003). Moreover, it remains unclear whether lithosphere thinning can lead to the development of deep faults, or in contrast, whether extension of the lithosphere owe their existence to activities of deep faults (Wang et al., 2006, 2007; Wu et al., 2003; Xu et al., 1993).

As an important tectonic boundary belt of South China, the Gan–Hang Tectonic Belt (GHTB) provides an excellent opportunity to study and potentially resolve the controversies outlined above. Thus, in this paper, we present new analytical data for two representative mafic–ultramafic intrusions in the GHTB. Combined with previously published geochemical data, our new results provide constrains on the petrogenesis of these rocks, and their tectonic significance, and help to understand the lithospheric evolution and geodynamics of South China.

2. Geological setting

As an important active tectonic–magmatic belt, the GHTB is located at the junction of the Yangtze Block and the Cathaysia Block. It has gone through several tectonic overprinting events (structural, magmatic, and metamorphic) and contains widespread mineralization (Deng and Zhang, 1989; Deng and Zheng, 1997, 1999; Goodell et al., 1991; Zhang, 1999). The belt comprises several components that are delineated by three deep, large-scale fault systems: the Yongfeng–Fuzhou Fault, the Dongxiang–Guangfeng Fault, and the Jiangshan–Shaoxing Fault (see Fig. 1, Yu et al., 2006). They form the western, the middle, and the eastern sections of GHTB, respectively. From west to east, there are also three basins in GHTB: the Fuzhou–Chongren Basin, the Xinjiang Basin, and the Jinhua–Quzhou Basin (Fig. 1).

In the study area, Mesoproterozoic to Cenozoic sedimentary rocks exhibit regional differences that are related to the tectonic activity. The GHTB underwent three periods of large-scale extension: (i) lithospheric stretching in relation to Tungwu movement during the Permian, which resulted in the formation of the Yongfeng–Zhuji depression; (ii) a further period of extension during the Late Jurassic which caused the formation of the Gan–Hang volcanic belt; and (iii) extensional tectonics at the end of the Early Cretaceous which culminated in the development of the Gan–Hang graben-bound basins (Yu et al., 2006). The latter two periods of extension were large-scale events that occurred during the Yanshanian Epoch (~195–65 Ma) and constitute the main periods of tectonic activity in the GHTB (Yu et al., 2006). These events also led to extensive magmatic activity, including the eruption of a bimodal basalt–rhyolite association, and the emplacement of granite, gabbro, and dolerite (Goodell et al., 1991). As such, a study of these igneous rocks provides an excellent opportunity to probe and systematically investigate the dynamic background of the GHTB.

The majority of mafic–ultramafic intrusions across the GHTB were emplaced into the Jurassic–Cretaceous strata, all along the main fault zones. The intrusions are predominantly composed of gabbro and olivine-gabbro, outcropping as annular-shaped bodies ranging from several square kilometers to tens of square kilometers. Columnar

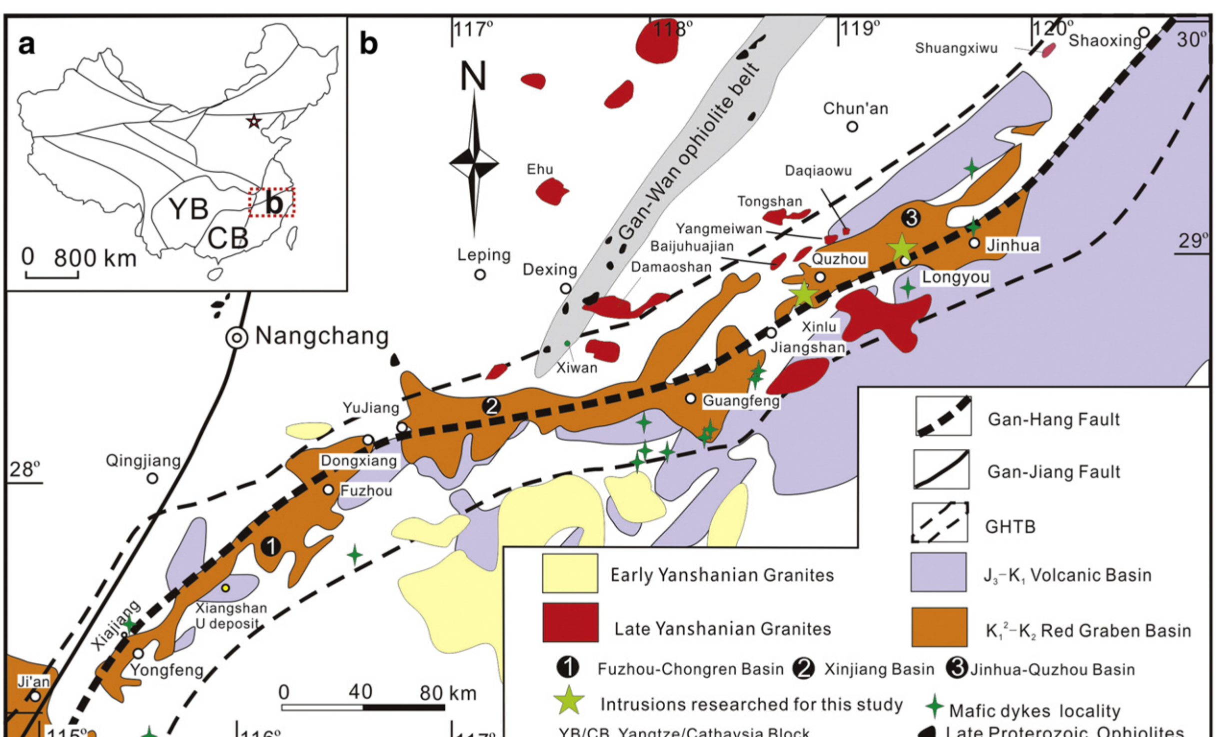

Fig. 1. (a) Simplified map of China. (b) Geological map of the Gan–Hang tectonic belt (GHTB), South China, and sampling localities of mafic intrusions from the GHTB.

jointing is well developed in many of the mafic–ultramafic intrusions with joint fissures filled with quartz, indicating rapid intruding and cooling at a shallow crustal level. The locations of individual intrusions and dykes are shown in Fig. 1.

3. Sampling and analytical methods

Thirteen samples from Quzhou (HBM and JT) and ten samples from Longyou (HTSM and HT) were collected for study (see Fig. 1b). The sampled mafic–ultramafic rocks are predominantly dark green and exhibit typical gabbroic characters. The rocks are composed of plagioclase and clinopyroxene with minor olivine, orthopyroxene, and Ti-magnetite. Olvine is more abundant in samples from Longyou. The gabbros are porphyritic and contain ~35 % phenocrysts of clinopyroxene (0.2–0.5 mm), plagioclase (0.5–1.2 mm), and sometimes olivine (~0.5 mm). The groundmass consists of clinopyroxene, plagioclase, and magnetite, and the grain size is ~0.05 mm. Most plagioclase phenocrysts are labradorite ($An_{50–70}$) and are euhedral, whereas clinopyroxene phenocrysts (mainly augite) are commonly subhedral. Fig. 2 shows representative outcrops and photomicrographs of the rocks.

Whole-rock samples were trimmed to remove any weathered surfaces then powdered using an agate mill for major and trace elements and Sr–Nd isotopic composition measurements. Major oxides were analyzed with a PANalytical Axios-advance X-ray fluorescence spectrometer (XRF) at the State Key Laboratory of Ore Deposit Geochemistry (SKLODG), Institute of Geochemistry, Chinese Academy of Science (IGCAS), Guiyang, China. Whole-rock trace elements, including rare earth elements (REEs), were analyzed using a Perkin-Elmer ELAN 6000 inductively coupled plasma–mass spectrometer (ICP–MS) at IGCAS using the analytical procedures outlined in Qi et al. (2000). Precision and accuracy range from 5% to 10% for all elements. The results of both XRF and ICP–MS analyses are presented in Table 1.

Zircons were separated from crushed rocks of JT and HTSM using heavy liquid and magnetic separation techniques and then carefully handpicked under a binocular microscope. Zircon grains were mounted in epoxy resin and were then polished. In order to reveal the internal textures and zonation of zircons, polished sections were carbon coated and then cathodoluminescence (CL) imaging was conducted at the State Key Laboratory of Continental Dynamics, Northwest University, Xi'an, China.

Zircons were dated using Laser ablation ICP–MS methods, with the Agilent 7500a ICP–MS equipped with 193 nm excimer lasers at the State Key Laboratory of Geological Processes and Mineral Resources, China University of Geoscience in Wuhan, China, following the analytical procedures outlined in Liu et al. (2008a, 2010a, 2010b). Off-line selection and integration of background and analyte signals and time-drift correction and U–Pb dating were performed using *ICPMSDataCal* (Liu et al., 2008a, 2010a,b). Zircon 91500 was used as the extrerns standard. Common Pb corrections were made using the method of Andersen (2002). Data plotting and age calculation were done using ISOPLOT (Ludwig, 2003). Errors on individual analyses by LA–ICP–MS are quoted at the 95% confidence level.

Sr–Nd isotopic measurements were performed using a MAT-262 TIMS instrument at the Institute of Geology and Geophysics, Chinese Academy of Science (IGGCAS), Beijing, China. The analytical procedures and experimental conditions were the same as documented in Liu et al. (2008b). Procedural blanks were controlled below 100 pg for Sm and Nd, and 500 pg for Rb and Sr. The mass fractionation corrections for Sr and Nd isotopic ratios were based on $^{86}Sr/^{88}Sr = 0.1194$ and $^{146}Nd/^{144}Nd = 0.7219$, respectively. Analyses of standards during the period of analysis were as follows: NBS987 with $^{87}Sr/^{86}Sr = 0.710263 \pm 11$ (2σ); Jndi-1 with $^{143}Nd/^{144}Nd = 0.512113 \pm 13$ (2σ).

4. Analytical results

4.1. Zircon U–Pb ages

Euhedral zircon grains of samples JT01-1 from Quzhou and HTSM from Longyou are prismatic, with magmatic oscillatory zoning (Fig. 3). Eight grains from sample JT01-1 have a weighted mean $^{206}Pb/^{238}U$ age of 126.2 ± 2.4 Ma (95% confidence level; Table 2 and Fig. 3), whereas eleven zircon grains from sample HTSM have $^{206}Pb/^{238}U$ ages that cluster between 120 and 138 Ma and registered a weighted mean age of 129.0 ± 3.9 Ma (95% confidence level) (Table 2 and Fig. 3). These dating results significantly overlap in their 95 confidence level range.

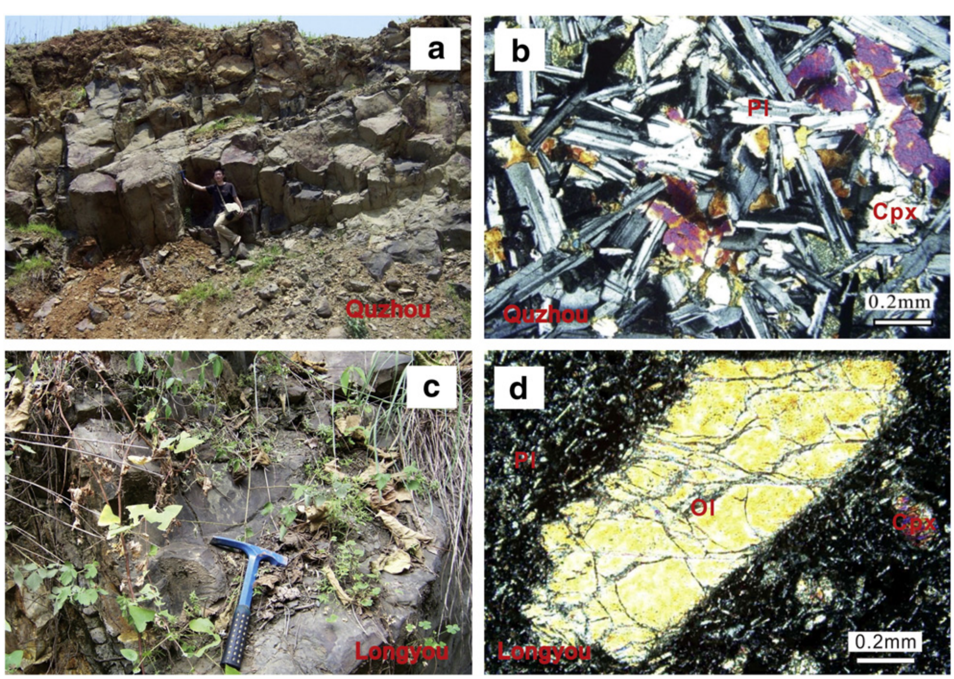

Fig. 2. Field photographs of mafic intrusions in Quzhou (a) and Longyou (c). Representative photomicrographs of mafic intrusions from Gan–Hang tectonic belt (GHTB), South China: (b) for Quzhou; and (d) for Longyou. Cpx, clinopyroxene; Pl, plagioclase; Ol, olivine.

Table 1
Major oxides (wt.%) and trace elements (ppm) for the representative mafic–ultramafic intrusions in GHTB, South China.

Sample No.	JT01-2	JT01-3	JT01-4	HBM1	HBM2	HBM3	HBM4	HBM5	HBM6	HBM7	HBM8	HBM9	HBM10	HT1	HT2	HTSM1	HTSM2	HTSM3	HTSM4	HTSM5	HTSM6	HTSM7	HTSM8
Locality	Quzhou													Longyou									
SiO_2	50.24	48.94	50.62	51.79	50.30	51.03	50.78	49.81	50.85	51.21	50.50	50.52	50.09	42.28	45.11	42.95	43.10	41.99	41.50	42.92	42.18	43.25	41.75
TiO_2	2.21	2.23	2.29	2.32	2.28	2.25	2.26	2.32	2.30	2.28	2.29	2.23	2.26	2.58	2.35	2.53	2.53	2.58	2.57	2.51	2.60	2.56	2.59
Al_2O_3	14.93	14.85	14.90	15.16	14.87	14.73	14.95	15.06	14.90	15.09	14.90	14.76	14.66	12.27	12.61	12.18	12.26	12.20	12.10	12.11	12.24	12.26	12.15
Fe_2O_3	11.56	11.25	10.62	11.23	10.64	11.24	10.78	10.48	10.50	11.14	10.79	11.10	10.81	12.61	12.14	12.51	12.54	12.42	12.21	12.44	12.57	12.62	12.49
MnO	0.15	0.15	0.15	0.15	0.15	0.15	0.15	0.13	0.16	0.14	0.16	0.15	0.14	0.18	0.17	0.17	0.17	0.17	0.18	0.17	0.18	0.17	0.18
MgO	6.99	6.07	6.74	6.70	6.62	7.21	7.08	6.30	6.71	6.45	6.82	6.71	6.82	9.90	9.28	9.90	9.79	9.32	9.05	9.77	9.87	9.65	9.64
CaO	8.27	8.54	8.71	8.42	8.50	8.20	8.54	8.62	8.81	8.42	8.65	8.35	8.37	9.74	8.64	9.46	9.46	9.72	10.07	9.45	9.77	9.61	9.75
Na_2O	3.27	3.09	3.25	3.42	3.19	3.31	3.24	3.11	3.24	3.33	3.24	3.27	3.18	4.90	4.53	5.08	5.06	4.69	4.75	4.76	5.04	5.05	4.92
K_2O	0.67	0.56	0.64	0.62	0.65	0.62	0.65	0.58	0.64	0.61	0.63	0.59	0.63	1.57	1.75	1.41	1.38	1.45	1.47	1.54	1.42	1.32	1.42
P_2O_5	0.30	0.26	0.27	0.26	0.27	0.25	0.27	0.27	0.27	0.25	0.27	0.25	0.26	1.09	0.97	1.03	1.03	1.09	1.08	1.02	1.11	1.04	1.09
LOI	1.35	2.74	1.78	1.21	2.05	1.02	1.58	3.17	1.81	1.49	1.71	0.99	1.68	2.84	2.46	2.94	2.45	3.11	4.71	2.66	2.75	2.62	2.97
Total	99.94	98.68	99.97	101.28	99.52	100.00	100.28	99.85	100.19	100.40	99.96	98.91	98.90	99.96	100.01	100.16	99.77	98.74	99.69	99.34	99.73	100.15	98.95
Fe/Mn	68.4	66.5	63.9	68.8	64.1	69.5	64.9	72.8	59.3	71.4	60.9	68.8	69.7	63.3	64.2	67.3	67.5	66.0	61.3	67.5	63.1	67.6	62.7
$Mg^{\#}$	54.5	51.7	55.7	54.2	55.2	56.0	56.5	54.4	55.9	53.4	55.6	54.5	55.6	60.9	60.2	61.1	60.7	59.8	59.5	60.9	60.9	60.2	60.5
Ba	252	283	229	200	211	197	200	205	222	210	219	206	213	851	884	825	854	835	872	834	825	941	847
Rb	21.4	16.7	15.9	17.7	17.9	18.1	17.3	16.5	17.7	16.4	16.0	15.6	16.9	48.9	55.5	56.9	61.7	62.0	46.7	66.4	59.4	49.3	57.7
Sr	453	378	379	325	361	317	340	374	368	346	361	331	347	1150	1204	1160	1210	1140	1140	1180	1140	1150	1140
Y	25.0	24.1	24.3	23.0	25.0	23.3	23.3	24.7	25.0	23.8	23.9	23.6	24.0	26.9	26.9	25.0	25.7	27.0	26.0	25.6	25.7	25.6	26.3
Zr	197	167	180	151	184	151	172	181	183	154	176	152	180	298	315	247	255	294	291	255	292	254	293
Nb	20.4	15.0	15.3	16.9	16.4	16.4	15.3	15.7	15.8	16.3	15.0	15.9	15.7	102.6	110.8	113.0	116.0	101.0	98.7	115.0	98.7	116.0	99.5
Th	2.2	1.7	1.5	1.5	1.6	1.5	1.6	1.6	1.6	1.4	1.6	1.5	1.5	10.0	10.5	9.1	9.4	9.4	9.3	9.6	9.8	9.4	9.9
Zn	162	150	128	158	156	135	122	132	163	164	138	166	126	152	163	154	151	154	152	175	142	159	150
Ni	135	117	113	123	126	133	122	103	119	114	112	118	114	193	218	196	199	202	196	198	196	205	195
V	180	188	194	173	195	168	180	202	200	171	191	172	193	166	144	141	146	173	168	143	161	146	165
Cr	220	213	182	199	194	209	191	193	190	181	181	187	188	223	238	203	220	228	220	210	213	212	215
Hf	4.97	4.59	4.51	3.52	4.52	3.54	4.28	4.57	4.36	3.85	4.45	3.55	4.04	6.57	6.92	5.25	5.28	6.24	6.22	5.28	6.24	5.32	6.17
Sc	18.9	19.2	21.2	17.3	21.4	17.2	19.9	22.5	22.8	17.4	20.6	17.5	20.8	21.0	17.1	16.4	17.8	21.8	21.2	17.2	20.4	16.8	20.9
Ta	1.35	0.97	0.79	0.96	0.89	0.93	0.76	0.83	0.80	0.90	0.83	0.90	0.83	5.42	6.44	6.12	6.26	5.11	5.02	6.26	5.11	6.38	5.25
Co	45.3	41.9	79.3	40.1	87.3	41.3	72.4	63.5	78.5	41.1	83.5	39.6	83.1	73.5	53.6	48.4	49.1	72.3	73.4	48.3	80.9	49.4	114.0
U	0.46	0.39	0.33	0.29	0.34	0.28	0.33	0.40	0.39	0.31	0.36	0.30	0.35	2.23	2.62	2.50	2.12	2.32	2.65	1.99	2.21	1.99	2.33
La	14.8	11.4	12.0	12.1	12.2	11.9	11.7	11.9	12.1	12.0	11.9	11.9	12.0	63.1	64.8	64.0	65.9	62.0	60.2	66.2	61.4	66.7	62.9
Ce	31.5	24.8	26.3	25.9	26.8	25.5	25.9	26.6	26.5	25.9	26.1	25.6	26.0	112.0	118.5	112.0	116.0	110.0	105.0	116.0	109.0	117.0	111.0
Pr	4.15	3.38	3.52	3.60	3.59	3.56	3.56	3.69	3.57	3.62	3.46	3.58	3.52	13.50	13.06	12.90	13.30	12.90	12.80	13.40	13.00	13.20	12.90
Nd	19.2	16.5	16.6	17.5	17.3	17.6	16.1	17.3	16.9	18.0	16.5	17.7	16.7	50.5	51.0	51.4	52.9	49.1	48.0	52.9	49.5	52.7	48.4
Sm	5.19	4.67	4.80	5.15	4.77	5.04	4.61	4.98	4.86	5.21	4.72	5.11	4.99	10.00	10.09	10.10	10.30	9.59	9.36	10.50	10.10	10.50	9.82
Eu	1.86	1.72	1.95	1.79	2.04	1.82	1.88	2.08	2.05	1.89	1.90	1.82	1.92	3.63	3.24	3.31	3.41	3.61	3.38	3.35	3.71	3.44	3.62
Gd	6.40	5.88	5.74	5.42	5.94	5.19	5.56	6.05	5.70	5.48	5.66	5.34	5.90	9.55	10.82	8.84	9.30	9.63	9.72	9.00	10.12	9.08	9.93
Tb	0.91	0.87	0.86	0.85	0.86	0.83	0.81	0.89	0.87	0.90	0.85	0.85	0.84	1.28	1.22	1.21	1.26	1.23	1.21	1.27	1.25	1.29	1.25
Dy	5.23	4.97	4.69	4.60	4.63	4.54	4.30	4.87	4.66	4.68	4.52	4.60	4.53	5.56	6.35	5.52	5.64	5.80	5.66	5.63	5.69	5.69	5.72
Ho	0.97	0.93	0.91	0.89	0.88	0.91	0.81	0.93	0.88	0.94	0.86	0.89	0.90	0.99	1.06	0.98	1.00	0.96	0.94	1.01	0.99	1.00	0.95
Er	2.52	2.34	2.28	2.18	2.33	2.20	2.20	2.41	2.25	2.25	2.25	2.19	2.31	2.43	2.62	2.24	2.28	2.39	2.30	2.33	2.38	2.35	2.34
Tm	0.34	0.31	0.32	0.29	0.30	0.29	0.30	0.32	0.31	0.28	0.30	0.29	0.31	0.28	0.31	0.27	0.25	0.28	0.28	0.28	0.28	0.27	0.30
Yb	2.01	1.95	1.86	1.75	1.82	1.69	1.76	1.80	1.80	1.79	1.83	1.82	1.81	1.66	1.82	1.48	1.50	1.54	1.57	1.59	1.57	1.55	1.57
Lu	0.29	0.26	0.26	0.24	0.25	0.23	0.24	0.26	0.26	0.24	0.26	0.22	0.27	0.23	0.24	0.20	0.20	0.20	0.19	0.20	0.22	0.20	0.19
ΣREE	95.3	80.0	82.1	82.3	83.7	81.3	79.7	84.1	82.7	83.2	81.1	81.9	82.0	274.7	285.1	274.4	283.2	269.2	260.6	283.7	269.2	285.0	270.9
Rb/Sr	0.05	0.04	0.04	0.05	0.05	0.06	0.05	0.04	0.05	0.05	0.04	0.05	0.05	0.04	0.05	0.05	0.05	0.05	0.04	0.06	0.05	0.04	0.05
Nb/Ta	15.1	15.5	19.3	17.7	18.3	17.6	20.1	18.9	19.8	18.1	17.9	17.7	19.0	18.9	17.2	18.5	18.5	19.8	19.7	18.4	19.3	18.2	19.0
Zr/Hf	39.6	36.4	39.8	42.9	40.7	42.7	40.2	39.5	42.0	40.0	39.6	42.8	44.5	45.3	45.5	47.0	48.3	47.2	46.8	48.3	46.8	47.7	47.5
$(La/Yb)_N$	5.3	4.2	4.6	5.0	4.8	5.1	4.8	4.7	4.8	4.8	4.7	4.7	4.8	27.3	25.5	31.0	31.5	28.9	27.5	29.9	28.1	30.9	28.7
Sr/Y	18.1	15.7	15.6	14.1	14.4	13.6	14.6	15.1	14.7	14.5	15.1	14.0	14.5	42.8	44.8	46.4	47.1	42.2	43.8	46.1	44.4	44.9	43.3
Lu/Hf	0.06	0.06	0.06	0.07	0.06	0.06	0.06	0.06	0.06	0.06	0.06	0.06	0.07	0.03	0.03	0.04	0.04	0.03	0.03	0.04	0.04	0.04	0.03
Eu/Eu*	1.0	1.0	1.1	1.0	1.2	1.1	1.1	1.2	1.2	1.1	1.1	1.1	1.1	1.1	0.9	1.1	1.1	1.1	1.1	1.1	1.1	1.1	1.1

LOI, loss on ignition; $Mg^{\#} = 100 \times Mg / (Mg + \Sigma Fe)$ atomic ratio. $(La/Yb)_N = La_N / Yb_N$, normalized data after Sun and McDonald (1989).

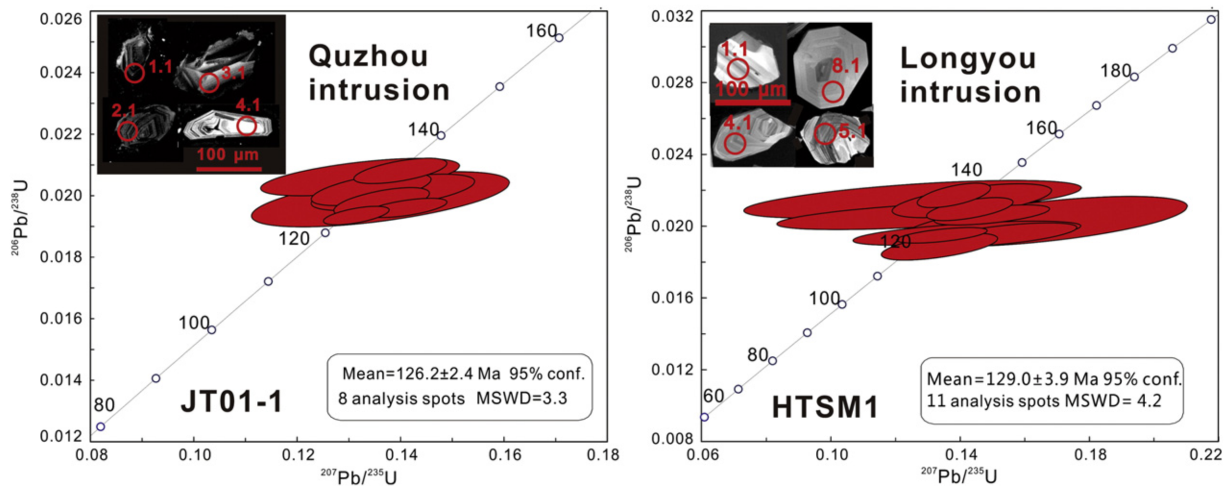

Fig. 3. Representative cathodoluminescence images and laser ablation–inductively coupled plasma–mass spectrometry (LA–ICP–MS) U–Pb Concordia diagrams for zircon grains from the gabbro samples.

4.2. Major and trace elements

Major element oxide and trace element concentrations are shown in Table 1. The samples exhibit a wide composition range as a whole but a quite narrow range for each intrusion (Table 1). The mafic rocks from Quzhou have relatively narrow ranges of SiO_2 (48.94–51.79 wt%), MgO (6.07–7.21 wt%), Fe_2O_3 (10.48–11.56 wt%), CaO (8.20–8.81 wt%), and $Mg^{\#}$ (51.7–56.5) with low K_2O (0.56–0.67 wt%) and Na_2O (3.09–3.42 wt%) relative to the ultramafic rocks. The ultramafic rocks from Longyou have distinct lower SiO_2 (41.50–45.11 wt%) and higher MgO (9.05–9.90 wt%), Fe_2O_3 (12.14–12.62 wt%), CaO (8.64–10.67 wt%), and $Mg^{\#}$ (59.5–61.1) with relatively higher K_2O (1.32–1.75 wt%) and Na_2O (4.53–5.08 wt%). In the total alkali-silica (TAS) diagram (Fig. 4), the samples from Quzhou fall within the fields of basalt with a subalkaline character based on the classification of Irvine and Baragar (1971). According the texture and content of K_2O and Na_2O, samples from Quzhou are middle-K calc-alkaline diabase. By contrast, the samples from Longyou fall within the fields of tephrite/basanite, with an alkaline character.

All studied rocks are characterized by enrichment in light rare earth elements and depletion in heavy rare earth elements, with $(La/Yb)_N$ values of 4.2–31.5 and Eu/Eu* of 0.9–1.2. Samples from Longyou have much higher $(La/Yb)_N$ ratios (25.5–31.5) than those from Quzhou (4.2–5.3). In Fig. 5, the composition range for volcanic rocks and mafic dykes from GHTB are shown with the yellow and blue shaded regions, respectively (Qi et al., 2012; Yu et al., 2006). In general, the data for volcanic rocks and the mafic dykes are much more variable than the intrusions.

In Primitive-mantle-normalized trace element diagrams, GHTB mafic–ultramafic intrusions are similar to those of OIB, being enriched in large ion lithophile elements (i.e., Rb, Ba, K, and Sr) and some high field strength elements (e.g., Nb, Ta,), but slightly depleted in Th, U, Ti, and Y (see Fig. 5b). All of the samples from Longyou show relative enrichment in Th and U. Nickel, Cr, and Co concentrations of the studied mafic–ultramafic intrusions range from 103 to 218 ppm, from 181 to 238 ppm, and from 39.6 to 144.0 ppm, respectively. Rocks from Longyou have relatively high contents of Ni and Cr, again consistent with their more primitive character. The correlation between MgO and SiO_2, TiO_2, CaO, Al_2O_3, Th, Sr, Ni, and Cr is shown in Fig. 6.

Table 2
LA–ICP–MS U–Pb isotopic data for zircons present within mafic–ultramafic intrusions of the GHTB, South China.

HTSM					Isotopic ratios						Age (Ma)					
Spot	Pb	Th	U	Th/U	$^{207}Pb/^{206}Pb$	1σ	$^{207}Pb/^{235}U$	1σ	$^{206}Pb/^{238}U$	1σ	$^{207}Pb/^{235}U$	1σ	$^{206}Pb/^{238}U$	1σ	$^{208}Pb/^{232}Th$	1σ
1.1	39	577	651	0.9\	0.0501	0.0036	0.1340	0.0093	0.0195	0.0003	128	8	124	2	123	4
2.1	28	465	261	1.8	0.0531	0.0086	0.1418	0.0234	0.0196	0.0004	135	21	125	3	131	5
3.1	9	128	116	1.1	0.0496	0.0120	0.1287	0.0303	0.0206	0.0005	123	27	131	3	132	8
4.1	10	137	150	0.9	0.0438	0.0127	0.1248	0.0346	0.0215	0.0007	119	31	137	4	120	10
5.1	15	218	214	1.0	0.0539	0.0046	0.1495	0.0118	0.0206	0.0004	141	10	132	2	137	5
6.1	9	131	80	1.6	0.0638	0.0125	0.1660	0.0292	0.0203	0.0009	156	25	129	6	143	10
7.1	27	366	431	0.8	0.0504	0.0032	0.1426	0.0089	0.0209	0.0004	135	8	134	3	144	5
8.1	19	307	232	1.3	0.0570	0.0053	0.1542	0.0143	0.0195	0.0004	146	13	125	3	129	5
9.1	14	233	195	1.2	0.0524	0.0054	0.1332	0.0119	0.0188	0.0005	127	11	120	3	118	6
10.1	22	251	468	0.5	0.0472	0.0028	0.1377	0.0075	0.0217	0.0005	131	7	138	3	151	6
11.1	18	266	180	1.5	0.0482	0.0062	0.1432	0.0163	0.0214	0.0006	136	15	137	4	130	6
JT01-1																
1.1	47	252	496	0.5	0.0494	0.0016	0.1312	0.0042	0.0194	0.0002	125	4	124	1	127	3
2.1	39	549	573	1.0	0.0485	0.0020	0.1398	0.0060	0.0208	0.0003	133	5	133	2	144	4
3.1	18	81	120	0.7	0.0461	0.0040	0.1319	0.0127	0.0206	0.0004	126	11	131	3	130	7
4.1	25	444	310	1.4	0.0498	0.0023	0.1361	0.0061	0.0198	0.0003	130	5	126	2	124	4
5.1	20	56	780	0.1	0.0522	0.0020	0.1409	0.0052	0.0196	0.0002	134	5	125	1	196	10
6.1	90	481	340	1.4	0.0499	0.0038	0.1383	0.0105	0.0201	0.0004	132	9	128	2	143	4
7.1	21	100	111	0.9	0.0519	0.0072	0.1359	0.0165	0.0199	0.0006	129	15	127	4	134	8
8.1	20	90	245	0.4	0.0486	0.0029	0.1341	0.0077	0.0202	0.0003	128	7	129	2	135	7

Note: LA–ICP–MS, laser ablation–inductively coupled plasma–mass spectrometry. Errors are at the 1σ level; Common Pb was corrected using the method proposed by Andersen (2002).

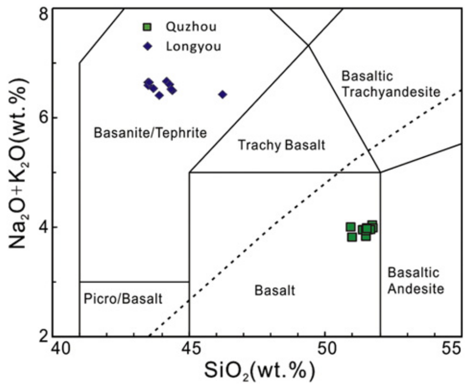

Fig. 4. A plot of total alkalis ($K_2O + Na_2O$) vs. SiO_2 exhibiting the various rock types for the mafic intrusions from GHTB, South China (reference fields are from Le Bas et al., 1986); the division between alkaline and subalkaline is after Irvine and Baragar (1971).

4.3. Sr–Nd isotopic compositions

The Sr and Nd isotopic compositions of the samples are listed in Table 3. These intrusions exhibit a range in $(^{87}Sr/^{86}Sr)_i$, $(^{143}Nd/^{144}Nd)_i$, and $\varepsilon_{Nd}(t)$ values from 0.70354 to 0.70554, from 0.51264 to 0.51281, and from +3.0 to +6.6, respectively. For comparison, Fig. 7 displays the isotopic results of this study along with data for other igneous rocks from GHTB and mafic rocks from South China (Chen and Wang, 1995; Ge et al., 2003; Li et al., 1990, 1997, 1998; Liu et al., 2004, 2008b, 2008c; Mao et al., 2006; Qi et al., 2012; Wang et al., 2003, 2004a, 2004b; Xie, 2003; Yan and Chen, 2007; Yu et al., 2004; Zhao, 2004; Zhou and Chen, 2001). All the isotopic data from mafic rocks of GHTB (area outlined with a black dotted line in Fig. 7) form an approximate linear trend from depleted mantle (DM) towards an enriched mantle II (EMII) composition, in which the investigated mafic–ultramafic intrusions trend towards DM compositions.

In $(^{87}Sr/^{86}Sr)_i$ versus $\varepsilon_{Nd}(t)$ diagram (Fig. 7), the data of the Cathaysia Block that includes Fujiang Province, Southern Jiangxi Province (Gannan for short) and Nouthern Guangdong Province (Yuebei for short) are mostly plotted above the GHTB data. On the contrary, the data of regions in Yangtze Block including Northern Jiangxi Province (Ganbei for short) and Shandong are generally plotted below the GHTB data. This pattern is consistent with the tectonic setting of GHTB being the boundary between the Cathaysia Block and the Yangtze Block. That is similar to the situation along the Chenzhou–Linwu Fault (Wang et al., 2003) that is in a similar tectonic boundary environment.

5. Discussion

5.1. Petrogenesis

5.1.1. Fractional crystallization

The relatively high contents of MgO = 6.07–9.90 wt.% and elevated $Mg^{\#}$ = 51.7–61.1 of the studied Mesozoic GHTB intrusions, together with the presence of clinopyroxene and olivine phenocrysts, indicate fractional crystallization of these two minerals. The relatively low contents of transition elements, such as Cr (181–238 ppm), Co (39.6–114.0 ppm), and Ni (103–218 ppm) compared with the contents of Primitive mantle (Cr: 2625 ppm; Co: 105 ppm; Ni: 1960 ppm; Rudnick and Gao, 2003), also indicate the fractionation of clinopyroxene and olivine. The much lower contents of Mg, Ni, Cr, and Co in the Quzhou intrusion relative to Longyou intrusion indicates that the former experienced more fractional crystallization. The absence of significant Eu anomaly and the slight enrichment of Sr in all of the samples suggest that plagioclase was not a major fractionating phase, which is consistent with petrographic observations.

Due to the narrow range content of MgO exhibited for each intrusions group, there are no obvious changes of TiO_2,CaO, Al_2O_3, Ni, Cr, Sr, and Th with decreasing MgO in Fig. 6. However, these data range of both intrusions are consistent or close to the data range of mafic dykes from GHTB. It indicates that our studied intrusions underwent same fractional crystallization of clinopyroxene and olivine with mafic dykes from GHTB (Qi et al., 2012). An exception is that less Cr content of Longyou ultramafic rocks, showing any fractionation of Cr-sipinel.

5.1.2. Crustal contamination

To assess the influence of low-temperature alteration and/or crustal contamination to samples is very important before speculating on their source. First, the petrographic observation of studied samples confirms that they are very fresh and free of significant alteration. In addition, the absence of reasonable correlations between Na_2O, K_2O, and LOI and the lack of a Ce anomaly suggest that the incompatible elemental and isotopic ratios have not been significantly affected by alteration (Deniel, 1998). The GHTB mafic–ultramafic rocks all display positive

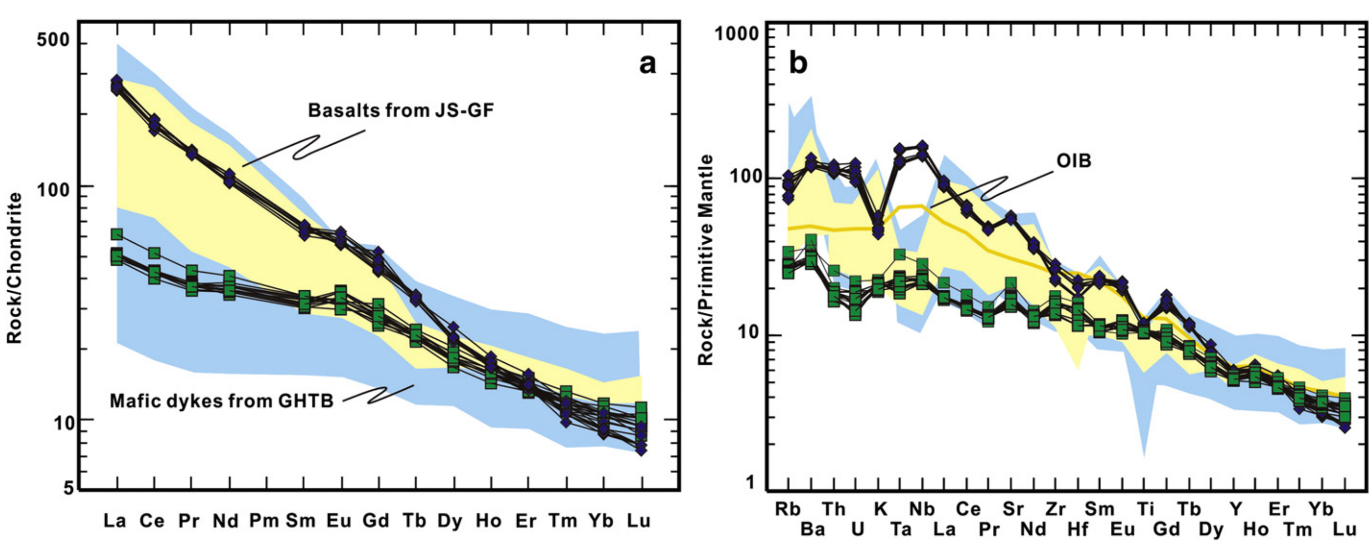

Fig. 5. (a) Chondrite-normalized rare earth element (REE) patterns and (b) primitive-mantle-normalized multi-element diagrams of mafic intrusions from GHTB, South China. REE abundances for chondrite and trace element abundances for primitive mantle are after Sun and McDonough (1989); the yellow and blue shaded areas are the range for volcanic rocks and mafic dykes from GHTB, respectively (data from Qi et al., 2012; Yu et al., 2006). JS-GF are shorten from Jiangshan and Guangfeng. Symbols are as in Fig. 4.

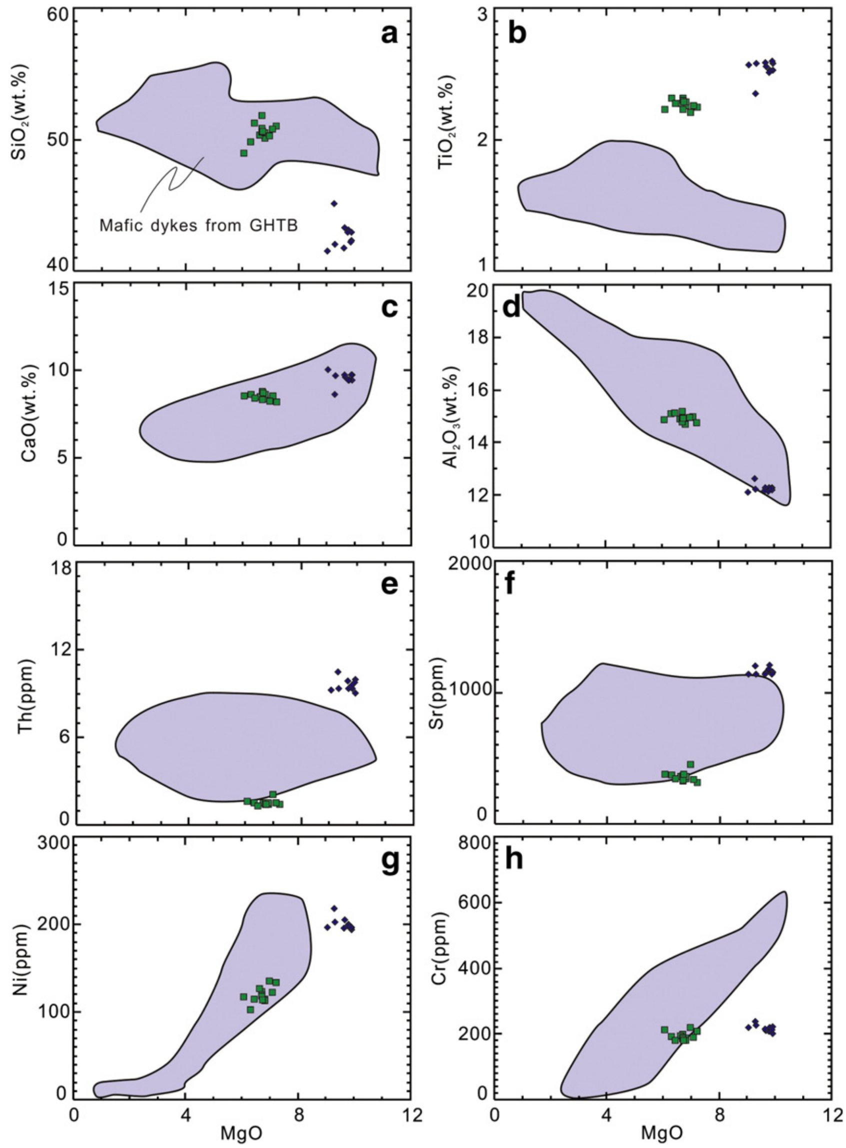

Fig. 6. Variation diagrams for select major oxides and trace elements versus MgO contents for mafic dykes from the Gan–Hang tectonic belt (GHTB), South China. (a) SiO_2 vs. MgO, (b) TiO_2 vs. MgO, (c) CaO vs. MgO, (d) Al_2O_3 vs. MgO, (e) Th vs. MgO, (f) Sr vs. MgO, (g) Ni vs. MgO, (h) Cr vs. MgO. Symbols are as in Fig. 4. Major oxides are in wt.% and trace elements in ppm.

Table 3
Sr–Nd isotope compositions for mafic–ultramafic intrusions of the GHTB, South China.

SAMPLE	$^{87}Rb/^{86}Sr$	$^{87}Sr/^{86}Sr$	$\pm 2\delta$	$^{87}Sr/^{86}Sr_i$	$^{147}Sm/^{144}Nd$	$^{143}Nd/^{144}Nd$	$\pm 2\delta$	$^{143}Nd/^{144}Nd_i$	$\varepsilon_{Nd}(t)$	Data
JT01-2	0.1365	0.70557	9	0.70533	0.1634	0.51279	2	0.51266	3.5	this study
JT01-3	0.1277	0.70576	5	0.70554	0.1711	0.51278	3	0.51264	3.2	
HBM1	0.1574	0.70548	6	0.70520	0.1779	0.51279	2	0.51264	3.2	
HBM3	0.1381	0.70534	11	0.70511	0.1765	0.51282	14	0.51268	3.9	
HBM7	0.1370	0.70568	4	0.70545	0.1750	0.51278	3	0.51264	3.0	
HBM9	0.1362	0.70555	4	0.70531	0.1745	0.51279	4	0.51265	3.3	
HT2	0.1332	0.70388	13	0.70364	0.1196	0.51284	12	0.51273	5.1	
HTSM2	0.1385	0.70385	11	0.70360	0.1194	0.51291	13	0.51281	6.6	
HTSM5	0.1626	0.70384	5	0.70354	0.1200	0.51287	2	0.51277	5.9	
HTSM7	0.1239	0.70381	4	0.70357	0.1204	0.51289	2	0.51278	6.2	
HTSM9	0.1463	0.70383	2	0.70355	0.1226	0.51288	1	0.51277	6.0	
GF03	0.1579	0.70877	14	0.70857	0.1040	0.51224	14	0.51217	-6.8	mafic dykes from Qi et al. (2012)
XJ01	0.2905	0.70464	13	0.70410	0.1943	0.51293	14	0.51276	5.6	
QB01	0.1080	0.70788	10	0.70773	0.1015	0.51233	11	0.51226	-4.9	
SXC2	0.3151	0.70703	13	0.70648	0.1278	0.51244	15	0.51233	-2.9	
YPF1	0.2463	0.70688	11	0.70642	0.1381	0.51247	16	0.51235	-2.3	
CXK4	0.3863	0.70850	11	0.70776	0.1193	0.51225	15	0.51215	-6.1	
HSY1	0.6441	0.71211	13	0.71103	0.1000	0.51203	14	0.51195	-10.4	
AD1	0.6066	0.70929	13	0.70869	0.1237	0.51230	14	0.51224	-5.9	

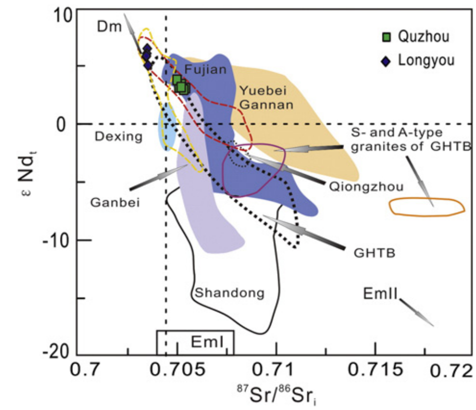

Fig. 7. Plot of initial ($^{87}Sr/^{86}Sr$) vs. $\varepsilon_{Nd}(t)$ value for the mafic intrusions from GHTB, South China. Area outlined with a black dotted line represents data for mafic dykes from GHTB in Late Mesozoic (Qi et al., 2012), whereas fields outlined with a yellow dashed line are Group 1 and red dashed line, Group 2 mafic rocks from the Yangtze and Cathaysia blocks, in the vicinity of the Chenzhou–Linwu Fault, respectively (Wang et al., 2003). Fujian data refers to Zhou and Chen (2001), Zhao (2004), and Mao et al. (2006); Yuebei and Gannan refers to Li (1990), Li et al. (1997), Li and McCulloch (1998) and Xie (2003); Qiongzhou refers to Ge et al. (2003); Ganhang refers to Chen and Wang (1995), Xie (2003), and Yu et al. (2004); S- and A-type granites of the GHTB are outlined with purple and brown lines, after Jiang et al. (2011); Ganbei refers to Xie (2003); Shandong refers to Liu et al. (2008a, 2008b) and Yan and Chen (2007); and Dexing refers to Wang et al. (2004a, 2004b). Symbols are as in Fig. 4.

$\varepsilon_{Nd}(t)$ values, accompanied by lower ($^{87}Sr/^{86}Sr$)$_i$ values, indicating that there were no contamination by crustal materials. Moreover, there are no obvious changes of Sr with decreasing MgO contents, which therefore excludes contamination by the lower crust, since crustal rocks have much lower Sr abundance (e.g., 350 ppm, Rudnick and Fountain, 1995). All the intrusions are characterized by relatively low Th (1.4–10.5 ppm) and U (0.28–2.65 ppm) contents when compared to the upper crust (e.g., Th = 10.5 ppm, U = 2.7 ppm; Rudnick and Fountain, 1995; Rudnick and Gao, 2003), thereby ruling out significant crustal contamination in the formation of these rocks. In summary, the magma evolution of the mafic–ultramafic intrusions from Quzhou and Longyou was not significantly affected by crustal contamination or alteration. Their geochemical and isotopic signatures are related to their mantle source(s).

5.1.3. Nature of the mantle source

The low SiO_2 contents (41.50–51.79 wt.%) of these rocks suggest that the mafic–ultramafic intrusions were derived from an ultramafic source and originated directly from the mantle (Liu et al., 2008b, 2008c, 2009).

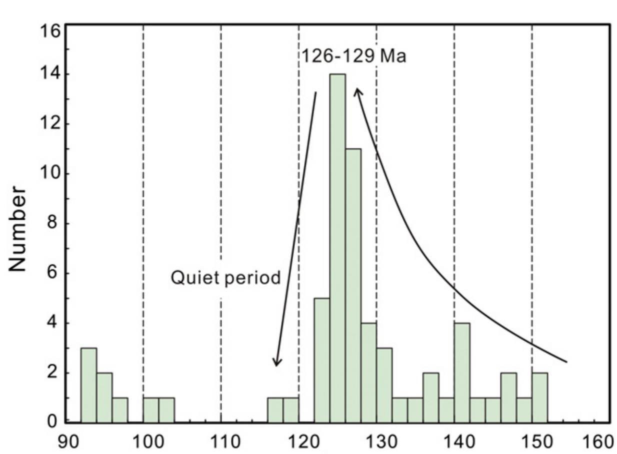

Fig. 8. Chronology histogram of Yanshanian plutonic rocks in GHTB and adjacent regions. Data for the ages are after Li et al. (2013). The range of ages from Longyou to Quzhou are consistent with the peak period of magmatism that occurred during 129–126 Ma.

In addition, the mafic–ultramafic intrusions of the GHTB have low ($^{87}Sr/^{86}Sr$)$_i$ value of 0.703535 to 0.705539 and high $\varepsilon_{Nd}(t)$ value of +3.0 to +6.6 (Table 3; Fig. 7), showing that they are much closer in composition to the depleted mantle (DM) source than other mafic dykes throughout the GHTB. This implies that these mafic–ultramafic intrusions originated from partial melting of a depleted mantle source such as an asthenospheric mantle or a relative juvenile SCLM (Zheng, 2012).

The crystallization of garnet can result in large LREE/HREE fractionation in the case of the low degree partial melting due to its preference to incorporating HREE. Both types of intrusions are characterized by relative depletion of HREE compared to the mafic dykes and basalts in GHTB in Fig. 5a, indicating the presence of residual garnet in their mantle source. The pressure of peridotite melting plays an important role on degree of silica saturation in basaltic magmas (Kushiro, 2001; Langmuir et al., 1992; Takahashi and Kushiro, 1983). Hence, it was proposed that low degrees of melting (<5% by weight) at high pressures (>3 GPa) could have produced alkalic magmas, such as the magma of the Longyou intrusion, whereas larger degrees of melting at shallow depths can generate tholeiitic or some calc-alkalic magmas such as those in the Quzhou intrusion (DePaolo and Daley, 2000; Hirose and Kushiro, 1993). However, the difference in degree of melting contradicts with the difference in Sr–Nd isotopes between the Longyou intrusion and the Quzhou intrusion (Fig. 7). The Quzhou intrusion has higher SiO_2 (48.49–50.51 wt %) but lower $\varepsilon_{Nd}(t)$ (+3.0 to +3.3) relative to the Longyou intrusion. Therefore, their differences cannot result from the different degree of peridotite melting. We propose that the differences were caused by near-solidus partial melting of pyroxenites with different content of silica (Hirschmann et al., 2003; Kogiso and Hirschmann, 2006; Kogiso et al., 2003; Pertermann and Hirschmann, 2003) instead.

Our hypothesis is supported by the Fe/Mn ratios. The Fe/Mn ratios for pyroxenite melts are higher than those for dry peridotite melts because $D_{Fe/Mn}$ values for clinopyroxene, orthopyroxene, and garnet are <1 but are >1 for olivine as shown by partial melting experiments (Pertermann and Hirschmann, 2003; Walter, 1998). Primitive upper mantle typically has a Fe/Mn ratio of 60 (Humayun et al., 2004), whereas pyroxenites in mantle have higher Fe/Mn ratios (Herzberg, 2006; Sobolev et al., 2007; Zhang et al., 2009). In this study area, both intrusions have Fe/Mn ratios of 59.3 to 72.8 (Table 3). They are higher than the ratios for typical primitive mantle (60) but close to the values for mantle proxenites; therefore, we infer that the Longyou and Quzhou magmas were produced by the partial melting of pyroxenites.

Coexisting silica-excess pyroxenites and silica-deficient pyroxenites may be produced in 2 settings: (1) In a subduction setting, silica-excess pyroxenites could result from the reaction of the mantle peridotite with granitic melts derived from subducting oceanic sediments (Zhang et al., 2009), whereas silica-deficient pyroxenites could be produced by the metasomatism of peridotite by adakitic melts (Herzberg, 2006; Rapp et al., 1999; Sobolev et al., 2007; Yaxley, 2000) generated from the partial melting of the dehydrated metabasalt (eclogite) (Defant and Drummond, 1990; Rapp et al., 1991, 2003. (2) In an intraplate setting, pyroxenites with various silica content may be produced by the metasomatism of peridotite by small melt fractions that are considered to be silica-rich and enriched in volatiles and incompatible elements in growing juvenile lithosphere above the lithosphere–asthenosphere interface (Niu and O'Hara, 2009).

In this study area, the OIB-like patterns of trace element distributions (Fig. 5) show enrichment in HFSE (Nb, Ta, Zr, Hf) relative to the neighbor elements, especially much more enrichment of HFSE in Longyou intrusion (lower SiO_2) compared with Quzhou intrusion. Such features suggest that the source rocks underwent dehydration before partial melting, resulting in depletion of water-soluble elements (e.g., Rb and Sr) rather than water-insoluble elements (e.g., Nb and Ta). This may contradict the situation of metasomatism of small melt fractions from the asthenosphere. Therefore, we infer that mafic–ultramafic rocks were likely produced in a subduction setting.

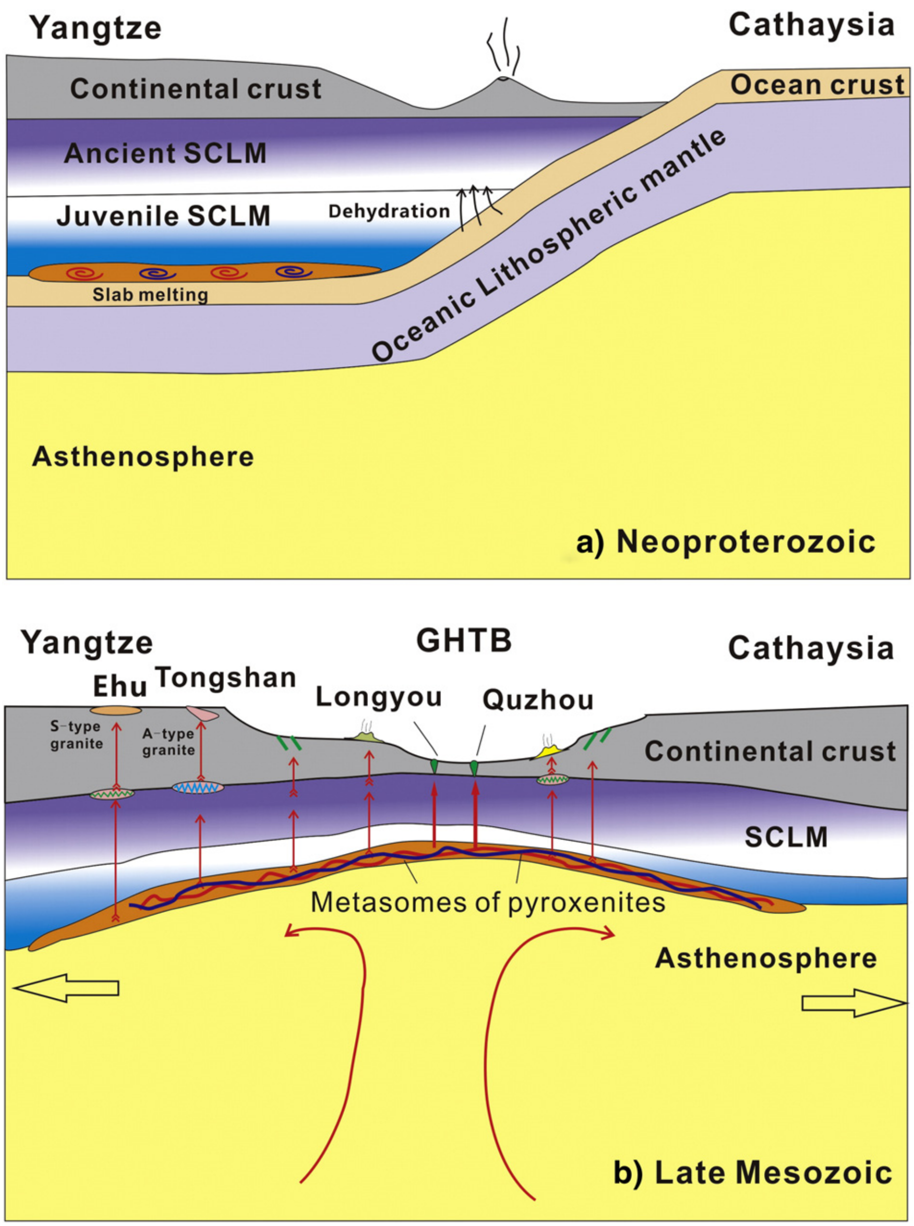

Fig. 9. Cartoon illustrating a petrogenetic model of oceanic crust-lithospheric mantle interaction for mafic intrusions in the GHTB, South China. (a) Neoproterozoic subduction of the oceanic crust from Cathaysia to Yangtze Block transformed the overlying mantle wedge to the juvenile SCLM. Then the adakitic and felsic melts resulted from partial melting of the dehydrated oceanic metabasalt and metasediment would ascend rapidly and react with the overlying juvenile SCLM peridotite to form the silica-deficient and silica-excess pyroxenites, respectively. (b) Late Mesozoic, the metasomes mainly composed of the silica-deficient and silica-excess pyroxenites, melted after their storage at the base of the SCLM for hundreds of millions of years. The partial melting of the pyroxenites was triggered during the peak extensional tectonics in response to the tectonic reactivation of GHTB in the Early Cretaceous. The mafic magma was finally emplaced into the shallow crust and crystallized.

As mentioned above, granitic and adakitic melts can be produced by partial melting of subducted oceanic sediments and dehydrated metabasalt (ecologite) (Defant and Drummond, 1990; Rapp et al., 1991, 2003; Zhang et al., 2009). The two types of melt have a relatively enriched and depleted signal in Sr–Nd isotope compositions, respectively. Their isotopic signatures could be inherited by different pyroxenites prodeced by their reaction with peridotite.

Regarding the studied mafic–ultramafic rocks in GHTB, the mixing between isotopically depleted silica-deficient pyroxenite magma and isotopically enriched silica-excess pyroxenite magma could well explain the gradual variations in radiogenic isotope compositions in association with major element abundances. We infer that GHTB and its peripheral region is in a subduction setting with an oceanic crust beneath the continental lithosphere (Zhao et al., 2015; Zheng, 2012). The same scenario is suggested to explain the petrogenesis of Cenozoic continental basalts in east-central China (Zhang et al., 2009).

Regarding the subducting oceanic crust, there is a tendency to think that it was the paleo-Pafic Plate. We don't think the subduction of the paleo-Pacific Plate would cause such a wide-ranging in magmatism in Late Mesozoic and Cenozoic. The ages of intrusions and volcanics in GHTB do not show a regular younging trend from the coast to the inland, as would be expected in response to subduction and possibly a subsequent "roll-back" (Li and Li, 2007). In fact, during the Late Mesozoic to Early Cenozoic, mafic rocks intruded all across the central Jiangxi Province, which was inland in SCB in the period of 49–65 Ma (Xie et al., 2005b), suggesting that their emplacement cannot simply be explained by subduction of the paleo-Pacific Plate. Some studies even postulated that subduction of the paleo-Pacific Plate was actually north–northeastward during the Late Mesozoic (Kimura et al., 1990;

Maruyama and Send, 1986; Ratschbacher et al., 2000), which would provide little opportunity for the development of back-arc extensional tectonics in our study region. It is very important that no island arc magmatism has been identified in southeast China to support the subduction of paleo-Pacific Plate.

Therefore, we speculate that the relative juvenile SCLM were probably not related to the subduction of paleo-Pacific plate in Mesozoic. A relatively early subduction in GHTB may be an alternative explanation. This is supported by recent research. Through comprehensive study on the ore-forming granodioritic porphyry in the Dexing porphyry copper deposit, Liu et al. (2012) proposed that the intrusion is a product of partial melting of the relict island arcs which formed in oceanic slab subduction in the early Neoproterozoic. The remnants were preserved then remelted to form fertile magmas in the Middle Jurassic.

The oceanic crust in Neoproterozoic should be considered more carefully according to the geological history in GHTB. It is believed that the Yangtze and Cathaysia Block amalgamated during the Neoproterozoic Sibao orogeny (also called the "Jiangnan" or "Jinning" orogeny in different literatures, Li et al., 2009), although the timing and evolution of Sibao orogeny are still controversial. The existence of ca. 1000 Ma ophiolite in the northeast-trending Gan–Wan ophiolite belt north of GHTB (see Fig. 1), and along the eastern extension of the Sibao orogen, suggests that new oceanic crust was being generated in the early Neoproterozoic (Chen et al., 1991; Li et al., 1994, 2002). Li et al. (2009) demonstrated that the Shuangxiwu volcanic rocks represent an assemblage of arc volcanism formed on the eastern segment of the Sibao orogen at ca. 970–890 Ma, prior to the final amalgamation between the Yangtze and the Cathaysia Blocks, then they constrained the period of subduction with the ages of the Xiwan adakitic granites, which average 968 ± 23 Ma (Li and Li, 2003), and obduction-type biotite granites, which average 880 ± 19 Ma (Li et al., 2008). Research of Zhao et al. (2011) showed that the ≥830 Ma mafic rocks along the southeastern margin of the Yangtze Block have arc-affinity geochemical characters, whereas mafic rocks younger than 830 Ma have compositions more typical of ocean island basalt. They suggested that the amalgamation of the Yangtze Block and Cathaysia Blocks should have occurred at ca. 830 Ma, with back-arc spreading occurring above the long-lived (950–735 Ma) oceanic subduction zone along the northern and western margin of the Yangtze Block.

In the period between Late Neoproterozoic and Early Mesozoic, many evidences support that the whole SCB was stable, which good for the preservation of the metasome formed in Neoproterozoic. It has been suggested that the Yangtze and Cathaysia Block underwent a similar geodynamic driver/setting since they amalgamated together. Moreover, there is no evidence supporting the presence of a Phanerozoic ocean within the SCB (Wang et al., 2013a, 2013b). Minor mafic magmatisms are reported in SCB in the period and are thought to be indicative of an abnormal heat source in deep lithosphere mantle (Dai et al., 2008). In addition, to access the influence on isotopic characteristics by the preservation, we made a simple simulated calculation and find that the low $(^{87}Sr/^{86}Sr)_i$ and high $\varepsilon_{Nd}(t)$ values can be derived from the juvenile pyroxenite that formed in Neoproterozoic.

In summary, it most likely involved dehydrated oceanic metabasalt and overlying metasediment partially melting to generate adakitic and felsic melts, respectively. Then the two types of melt reacted with the juvenile SCLM peridotite to form isotopically relatively depleted silica-deficient to enriched silica-excess pyroxenites. The two kinds of pyroxenites could partially melt in response to mantle upwelling that produced the lithosphere rifting in the Early Cretaceous, producing not only the alkalic igneous rock but also the calc-alkalic rocks in GHTB (Qi et al., 2012; Yu et al., 2004), and the intermediate-felsic rocks after the underplating of these melts into the middle-lower crust (Chen and Wang, 1995).

5.1.4. Mantle metasomatism

Metamorphic dehydration in subduction zones are common with increasing P–T conditions. These processes lead to the metasomatism of crustally derived felsic fluid/melt to the mantle wedge then convert olivine to pyroxene (Kelemen et al., 1992, 1998; Zheng, 2012). Mantle peridotite can also be metasomatized by mafic melts in "modal metasomatism" (Niu and O'Hara, 2009). In this case, hydrous minerals such as amphibole and phlogopite are generated from fluid percolation and metasomatic reactions in originally 'dry' peridotites, and the reaction involves mineralogical changes in peridotites (Ionov et al., 1997).

Geochemical features of the studied mafic–ultramafic intrusions suggest that they were derived from an LILE- and LREE-enriched mantle source modified through metasomatism. Volatile-bearing minerals (amphibole, mica and apatite) can play a major role in creating asthenoshpheric sources enriched in incompatible lithophile elements. In general, amphibole and phlogopite are the most common volatile-bearing minerals in mantle rocks (e.g., Grégoire et al., 2000, Ionov et al., 1997), but apatite has rarely been identified in mantle rocks, though it may be more common than reported (O'Reilly and Zhang, 1995). It has been suggested that the significant content of LILE in mafic intrusions implied that phlogophite and amphibole are the major repositories for LILE in lithospheric mantle (e.g., Foley et al., 1996; Grégoire et al., 2000; Ionov et al., 1997). Compared to amphibole in mantle rocks, phlogopite is a much more important host for K, Rb and Ba, since the Rb/Sr ratio is much higher in phlogopite (Ionov et al., 1997). Melts from amphibole-bearing mantle sources typically have lower Rb/Sr ratios (<0.1) and higher Ba/Rb ratios (>20) than those from phlogopite-bearing mantle sources (Furman and Graham, 1999). In GHTB, mafic–ultramafic rocks have Rb/Sr ratios of 0.04 to 0.06, much less than 0.1, as shown in Table 1, which suggests that amphibole was predominant in the mantle-melt source for such rocks (Ionov et al., 1997).

Nb/Ta and Zr/Hf ratios typically are not affected by magmatic processes, owing to the similar geochemical behavior among the Nb and Ta and Zr and Hf element pairs (Jochum et al., 1986, 1989). Only in the presence of an unusual metasomatic assemblage, during the formation of the mantle source, their ratios may be modified (Guo et al., 2004). It has been suggested that rutile is the major phase to produce superchondritic Nb/Ta and Zr/Hf ratios in a melt, while low-Mg amphibole is perhaps the dominant phase for generating a melt with low Nb/Ta and high Zr/Hf ratios (Foley et al., 2002; Pfänder et al., 2007; Rudnick et al., 2000; Tiepolo et al., 2000). Clinopyroxene is thought important in the generation of slightly elevated Nb/Ta and high Zr/Hf ratios in a melt (Pfänder et al., 2007). Phlogopite is not expected to crystallize as a primary phase during OIB evolution and would, therefore, have minor effects on both ratios due to its low partition coefficients for all HFSE (Pfänder et al., 2007).

The Nb/Ta and the Zr/Hf ratios of chondrite are 19.9 ± 0.6 and 34.3 ± 0.3, respectively (Münker et al., 2003). The Quzhou mafic intrusion has Nb/Ta ratios of 15.1–20.1 which are therefore subchondritic (Table 1), whereas Zr/Hf ratios of 36.4–48.3 are superchondritic. These ratios suggest the possibility of low-Mg amphibole metasomatism of the source. By contrast, the Longyou ultramafic intrusion exhibits near-chondritic Nb/Ta ratios of 17.2–19.8 (Table 2), superchondritic Zr/Hf ratios of 45.3–48.3, and much higher Nb (98.7–116.0), Ta (5.02–6.44), and Zr (247.0–315.0) than the upper crust (Nb = 25 ppm, Ta = 2.2 ppm, Zr = 190 ppm, Rudnick and Fountain, 1995; Rudnick and Gao, 2003). Therefore, the feature of Longyou intrusive rocks may be related to dehydration before partial melting and an unstable rutile phase in mantle source.

5.2. Geodynamic significance

5.2.1. Implications of zircon U–Pb ages

The relatively consistent zircon ages of 126–129 Ma for Quzhou and Longyou mafic–ultramafic intrusions represent an important magmatic event. So far, only a few mafic rocks in GHTB have been reported with the age close to 126–129 Ma (Jiang et al., 2011; Qi et al., 2012). For example, a mafic dyke from Xiajiang in the western part of GHTB intruded at 131.6 Ma, and a diabasic dyke coexisting with felsic rocks (A- and S-type granites) in middle GHTB has emplacement ages of 128.5 Ma (Jiang et al., 2011; Qi et al., 2012). All the reported mafic rocks are emplaced along the main fault of GHTB, whereas many contemporary felsic rocks are widespread in GHTB and its peripheral region. Wang et al. (2013b) reported that felsic volcanic rocks interbedded with the Laocun Formation are dated at 128.8–135 Ma with a mean of 132 Ma, and those within the Huangjian Formation are dated at 136–129 Ma (mean: 127 Ma). Both formations occur in the Xinlu basin, about 30 km north of Quzhou intrusion (see Fig. 1). Moreover, the Xiangshan uranium deposit has $^{206}Pb/^{238}U$ ages between 135.1 ± 1.7 and 134.8 ± 1.1 Ma, with the U derived from the host rhyodacite and rhyodacitic porphyry rocks, respectively (Yang et al., 2010). Yang et al. (2012) studied the Yangmeiwan granite and the Daqiaowu granitic porphyry from the northeastern part of the GHTB in western Zhejiang Province, and by using LA–ICP–MS and SHRIMP U–Pb dating of zircon grains, obtained ages of 133–136 Ma for them. Li et al. (2013) reported zircon U–Pb age data, geochemical characteristics, and Sr–Nd isotopes for the Late Jurassic and Early Cretaceous granitoids from the northwestern Zhejiang Province in northwestern GHTB. Their results reveal two distinct episodes of the Yanshanian magmatism: granodiorites formed at 148.6 ± 1.1 Ma, whereas A-type granites have ages between 129.0 ± 0.6 Ma and 126.1 ± 1.1 Ma. They suggested that two distinct episodes occurred during a tectonic transition from the Late Jurassic (ca. 150 Ma) to Early Cretaceous (ca. 129–126 Ma).

By including the published age data of Li et al. (2013) and others outlined above, we have constructed an age histogram for magmatism within the GHTB and its adjacent regions. Fig. 8 shows an obvious age mode at 129–126 Ma. This age range is consistent with the ages of the mafic–ultramafic intrusions from Longyou to Quzhou and an intense extension occurring during this period. During this period, nearly all the mafic rocks are located in the main fault in GHTB, which suggests that structural constraints played an important role in petrogenesis and emplacement of the mafic–ultramafic magmas. The quiet period in Fig. 9 may have been caused by the vast thermal loss during the peak period and the ending of a stretching stage.

5.2.2. Petrogenetic model and significance

We speculate that the subduction of oceanic lithosphere between the Yangtze Block and the Cathaysia Blocks most likely existed in Neoproterozoic. The subducted slabs were stored in the deep mantle after the arc volcanism and ocean island basalt (OIB)-like magmatism, as indicated by Wang et al. (2013a,b). On the basis of the above observations and arguments, a multi-stage model is used to explain the petrogenesis of the mafic–ultramafic intrusions in GHTB. First, in Neoproterozoic, there was a low-angle subduction of oceanic crust from Cathaysia Blocks to Yangtze Block before the continental components collided (Li et al., 2002, 2009; Zhao et al., 2011). The low-angle subduction not only delaminated the lower part of the ancient SCLM into the asthenosphere but also transformed the mantle wedge overlying the subducted oceanic crust into a juvenile SCLM. Subsequently, the adakitic and felsic melts resulted from partial melting of the dehydrated oceanic metabasalt and metasediment, ascended rapidly, and react with the overlying juvenile SCLM peridotite to form the silica-deficient and silica-excess pyroxenites, respectively. Thus, the juvenile SCLM is bracketed by the ancient SCLM above and the pyroxenites below and was stored for hundreds of millions of years until the Late Mesozoic. Then partial melting of the pyroxenites was triggered during the peak extensional tectonics in response to the tectonic reactivation of GHTB in the Early Cretaceous. The mafic–ultramafic magmas were finally emplaced into the shallow surface and crystallized due to rapid cooling.

The GHTB is a deep lithospheric fault zone (Deng and Zhang, 1989; Deng and Zheng, 1997, 1999; Goodell et al., 1991; Zhang, 1999), and its deep fault would facilitate the rapid upward movement of partial melts thereby minimizing crustal assimilation and crystal fractionation en route. This may be the reason for the structurally defined distribution of mafic–ultramafic intrusions and dykes with a much narrower scale distribution than felsic rocks (A-, S- type granite and rhyolite). Felsic rocks could well have originated from the underplating of basaltic magma, and most of partial melts derived from the pyroxenites were consumed in the process of underplating. This would contain types of volcanic rocks in the Shixi Formation (119–128 Ma) and the Jiangde Group (115–134 Ma) in Jiangshan–Shaoxing region (Li et al., 2011; Liao et al., 1999; Wang et al., 2002; Yu et al., 2006, 2008; Zhou, 2000). Furthermore, South China Block is characterized by a series of large-scale, NE-trending fault systems, such as the Gan–Hang, Chenzhou–Lingwu, Zhenghe–Dapu, and Changle–Nanao faults (Li et al., 2003; Zhang et al., 2013). It has been inferred that the Yanshanian granites in Southeast China were the products of faulting-induced re-melting, and the formation of the syntectonic, deformed granites along the Changle–Nanao shear zone (Tong and Tobisch, 1996; Yui et al., 1996). Therefore, the NE-trending fault systems in other areas of SCB should be paid more attention.

The combination of such data has the following implications concerning the geodynamics of GHTB and its evolution:

(i) Deep fault activities within the tectonic belt can play a more important role than initially expected in terms of controlling melt composition and should be the focus of further study.
(ii) Multi-episodes of Mesozoic magmatism within the GHTB occurred in close response to regional tectonic activity. Under the Late Mesozoic lithospheric extension affected whole SCB, in the context of the regional scale, mafic magmatism was probably and easily triggered by the reactivation of deep faults.
(iii) Moreover, the formative process producing extension is still not clear, and the influence of Pacific plate cannot be directly ruled out. The large-scale basalts of 90–40 Ma age, formed along the main fault in East China, show NE-SW trend and parallel to the west margin of the Pacific (Xu, 2014). Further studies, such comparison of mafic–ultramafic rocks with different ages in South and East China, are required to examine the role of Pacific plate.

6. Conclusions

Based primarily on new geochronological, geochemical, and Sr–Nd isotopic studies of the sampled mafic–ultramafic intrusions from GHTB, the following conclusions can be drawn:

(1) Zircon U–Pb dating of zircon has shown that the Longyou and Quzhou mafic–ultramafic intrusions in GHTB were intruded between 129 and 126 Ma ago. The dating results are consistent with the peak of extension in the Early Cretaceous throughout GHTB.
(2) These intrusions have similarities to OIB-type mafic rocks, displaying enrichment in LREEs and large ion lithophile elements (i.e., Rb, Ba, K, and Sr) and high field strength elements (e.g., Nb, Ta), but slight depletions in Th, U, Ti, and Y, and weak to no Eu anomalies (Eu/Eu* of 0.87–1.09). The Late Mesozoic mafic–ultramafic intrusions with a range in $(^{87}Sr/^{86}Sr)_i$ of 0.7035 to 0.7055, $(^{143}Nd/^{144}Nd)_i$ of 0.51264 to 0.51281, and $\varepsilon_{Nd}(t)$ values of +3.0 to +6.6.
(3) Their magmas were principally derived from near-solidus partial melting of pyroxenites with different content of silica, and the pyroxenites were resulted from a relative juvenile SCLM peridotite metasomatized by adakitic and felsic melts under subducted oceanic crust-lithospheric mantle in Neoproterozoic.
(4) The partial melting of the pyroxenites was triggered during the peak extensional event in response to the tectonic reactivation of GHTB in the Early Cretaceous, with no significant crustal contamination en route. The fault reactivation and structural

constraints within the GHTB played an important role in magmatic evolution and should be the focus of further study.

Acknowledgments

This research was supported by grants from the National Nature Science Foundation of China (40903018), the West Light Foundation of the Chinese Academy of Sciences to Dr. Qi, the forefront projects to Dr. Qi and the 12th Five-Year Plan project of State Key Laboratory of Ore-deposit Geochemistry, Chinese Academy of Sciences (SKLODG-ZY125-05), the CAS/SAFEA International Partnership Program for Creative Research Teams "Intraplate Mineralization Research Team" (KZZD-EW-TZ-20), and the Science and Technology Foundation of Guizhou Province (no. [2009] 2248). We thank Prof. Meifu Zhou and Gavin W. Clarke for their help in the manuscript, and Prof. Jinhui Yang for his sound advice on our studies, and we are grateful to Prof. Zhaoshan Chang for his English polishing help to our manuscript.

References

Andersen, T., 2002. Correction of common lead in U–Pb analyses that do not report ^{204}Pb. Chemical Geology 192 (1–2), 59–79.
Charvet, J., Lapierre, H., Yu, Y.W., 1994. Geodynamic significance of the Mesozoic volcanism of southeastern China. Journal of Southeast Asian Earth Sciences 9 (4), 387–396.
Chen, J.F., Jahn, B.M., 1998. Crustal evolution of southeastern China: Nd and Sr isotopic evidence. Tectonophysics 284 (1–2), 101–133.
Chen, F.R., Wang, D.Z., 1995. Comparative anatomy of two contrasting Mesozoic volcanic-intrusive complexes in NE Jiangxi and its vicinities, China. Geochimica 24 (2), 169–179 (in Chinese).
Chen, W.F., Chen, P.R., Xu, X.S., Zhang, M., 2005. Geochemistry of Cretaceous basaltic rocks in South China and the restriction on subduction of the Pacific plate. Science in China: D 35 (11), 1007–1018 (in Chinese).
Chen, J., Foland, K.A., Xing, F., Xu, X., Zhou, T., 1991. Magmatism along the southeast margin of the Yangtze block: Precambrian collision of the Yangtze and Cathaysia block of China. Geology 19, 815–818.
Dai, B.Z., Jiang, S.Y., Jiang, Y.H., Zhao, K.D., Liu, D.Y., 2008. Geochronology, geochemistry and Hf–Sr–Nd isotopic compositions of Huziyan mafic xenoliths, southern Hunan Province, South China: petrogenesis andimplications for lower crust evolution. Lithos 102, 65–87.
Defant, M.J., Drummond, M.S., 1990. Derivation of some modern arc magmas by melting of young subducted lithosphere. Nature 347, 662–665.
Deng, J.R., Zhang, Z.P., 1989. Gan–Hang tectonic belt and its geologic significance. Uranium Geology 5 (1), 15–21 (in Chinese).
Deng, J.R., Zheng, Z.P., 1997. Discussion on the Precambrian structural framework of the Gan–Hang Tectonic Belt. Uranium Geology 13 (6), 321–326 (in Chinese).
Deng, J.R., Zheng, Z.P., 1999. Discussion on regional geotectonic setting of Gan–Hang Tectonic Belt. Uranium Geology 15 (2), 71–76 (in Chinese).
Deniel, C., 1998. Geochemical and isotopic (Sr, Nd, Pb) evidence for plume-lithosphere interactions in the genesis of Grande Comore magmas (Indian Ocean). Chemical Geology 144 (3–4), 281–303.
DePaolo, D.J., Daley, E.E., 2000. Neodymium isotopes in basalts of the Southwest Basin and Range and lithospheric thinning during continental extension. Chemical Geology 169, 157–185.
Fan, W.M., Wang, Y.J., Guo, F., Peng, T.P., 2003. Mesozoic mafic magmatism in Hunan-Jiangxi province and the lithospheric extension. Earth Science Frontiers 10 (3), 159–169 (in Chinese).
Foley, S.F., Jackson, S.E., Fryer, B.J., Greenouch, J.D., Jenner, G.A., 1996. Trace element partition coefficients for clinopyroxene and phlogopite in an alkaline lamprophyre from Newfoundland by LAM–ICP–MS. Geochimica et Cosmochimica Acta 60 (4), 629–638.
Foley, S.F., Tiepolo, M., Vannucci, R., 2002. Growth of early continental crust controlled by melting of amphibolite in subduction zones. Nature 417 (6891), 837–840.
Furman, T., Graham, D., 1999. Erosion of lithospheric mantle beneath the East African Rift system: evidence from the Kivu volcanic province. Lithos 48, 237–262.
Ge, X.Y., Li, X.H., Zhou, H.W., 2003. Geochronology, geochemistry and Sr–Nd isotopes of the Late Cretaceous mafic dike swarms in southern Hainan Island. Geochemica 32 (1), 11–20 (in Chinese).
Gilder, S.A., Gill, J., Coe, R.S., Zhao, X.X., Liu, Z.W., Wang, G.X., Yuan, K.R., Liu, W.L., Kuang, G.D., Wu, H.R., 1996. Isotopic and paleomagnetic constraints on the Mesozoic tectonic evolution of south China. Journal of Geophysical Research 101 (B7), 16137–16354.
Goodell, P.C., Gilder, S., Fang, X., 1991. A preliminary description of the Gan–Hang failed rift, Southeastern China. Tectonophysics 197 (2–4), 245–255.
Grégoire, M., Lorand, J.P., O'Reilly, S.Y., Cottin, J.Y., 2000. Armalcolite-bearing, Ti-rich metasomatic assemblages in harzburgitic xenoliths from the Kerguelen Islands: implications for the oceanic mantle budget of high-field strength elements. Geochimica et Cosmochimica Acta 64 (4), 673–694.
Guo, F., Fan, W.M., Wang, Y.J., Zhang, M., 2004. Origin of early Cretaceous calc-alkaline lamprophyres from the Sulu orogen in eastern China: implications for enrichment processes beneath continental collisional belt. Lithos 78 (3), 291–305.
Herzberg, C., 2006. Petrology and thermal structure of the Hawaiian plume from Mauna Kea volcano. Nature 444, 605–609.
Hirose, K., Kushiro, I., 1993. Partial melting of dry peridotites at high pressures: determinations of compositions of melts segregated from peridotite using aggregates of diamond. Earth and Planetary Science Letters 11, 477–489.
Hirschmann, M.M., Kogiso, T., Baker, M., Stolper, E.M., 2003. Alkalic magmas generated by partial melting of garnet pyroxenite. Geology 31, 481–484.
Hu, R.Z., Bi, X.W., Su, W.C., Peng, J.T., Li, C.Y., 2004. The relationship between uranium metallogenesis and crustal extension during the Cretaceous-Tertiary in South China. Earth Science Frontiers 11 (1), 153–160 (in Chinese).
Hu, R.Z., Bi, X.W., Zhou, M.F., Peng, J.T., Su, W.C., Liu, S., Qi, H.W., 2008. Uranium metallogenesis in South China and its relationship to crustal extension during the Cretaceous to Tertiary. Economic Geology 103 (3), 583–598.
Hua, R.M., Chen, F.R., Zhang, W.L., Lu, J.J., 2005. Three major metallogenic events in Mesozoic in South China. Mineral Deposits 24 (2), 99–107 (in Chinese).
Humayun, M., Qin, L., Norman, M.D., 2004. Geochemical evidence for excess iron in the mantle beneath Hawaii. Science 306, 91–94.
Ionov, D.A., Griffin, W.L., O'Reilly, S.Y., 1997. Volatile-bearing minerals and lithophile trace elements in the upper mantle. Chemical Geology 141 (3–4), 153–184.
Irvine, T.N., Baragar, W.R.A., 1971. A guide to the chemical classification of the common volcanic rocks. Canadian Journal of Earth Sciences 8 (5), 523–548.
Jiang, Y.H., Jiang, S.Y., Dai, B.Z., Liao, S.Y., Zhao, K.D., Ling, H.F., 2009. Middle to late Jurassic felsic and mafic magmatism in southern Hunan province, southeast China: implications for a continental arc to rifting. Lithos 107 (3–4), 185–204.
Jiang, Y.H., Zhao, P., Zhou, Q., Liao, S.Y., Jin, G.D., 2011. Petrogenesis and tectonic implications of Early Cretaceous S- and A-type granites in the northwest of the Gan–Hang rift, SE China. Lithos 121 (1–4), 55–73.
Jochum, K.P., McDonough, W.F., Palme, H., Spettel, B., 1989. Compositional constraints on the continental lithospheric mantle from trace elements in spinel peridotite xenoliths. Nature 340 (6234), 548–550.
Jochum, K.P., Seufert, H.M., Spettel, B., Palme, H., 1986. The solar-system abundances of Nb, Ta, and Y, and the relative abundances of refractory lithophile elements in differentiated planetary bodies. Geochimica et Cosmochimica Acta 50 (6), 1173–1183.
Kelemen, P.B., Dick, H.J.B., Quick, J.E., 1992. Formation of harzburgite by pervasive melt/rock reaction in the upper mantle. Nature 358, 635–641.
Kelemen, P.B., Hart, S.R., Bernstein, S., 1998. Silica enrichment in the continental upper mantle lithosphere via melt/rock reaction. Earth and Planetary Science Letters 164, 387–406.
Kimura, G., Takahashi, M., Kono, M., 1990. Mesozoic collision–extrusion tectonics in eastern Asia. Tectonophysics 181 (1–4), 15–23.
Kogiso, T., Hirschmann, M.M., 2006. Partial melting experiments of bimineralic eclogite and the role of recycled mafic oceanic crust in the genesis of ocean island basalts. Earth and Planetary Science Letters 249, 188–199.
Kogiso, T., Hirschmann, M.M., Frost, D.J., 2003. High-pressure partial melting of garnet pyroxenite: possible mafic lithologies in the source of ocean island basalts. Earth and Planetary Science Letters 216, 603–617.
Kushiro, I., 2001. Partial melting experiments on peridotite and origin of mid-ocean ridge basalts. Annual Review of Earth and Planetary Sciences 29, 71–107.
Langmuir, C.H., Klein, E.M., Plank, T., 1992. Petrological systematics of mid-ocean ridge basalts: constraints on melt generation beneath ocean ridge. American Geophysical Union Geophysical Monograph Series 71, 81–180.
Le Bas, M.J., Maitre, R.W.L., Streckeisen, A., Zanettin, B., 1986. A Chemical Classification of Volcanic Rocks Based on the Total Alkali-Silica Diagram. Journal of Petrology **27** (3), 745–750.
Li, W.X., Li, X.H., 2003. Adakitic granites within the NE Jiangxi ophiolites, South China: geochemical and Nd isotopic evidence. Precambrian Research 122, 29–44.
Li, Z.X., Li, X.H., 2007. Formation of the 1300-km-wide intracontinental orogen and postorogenic magmatic province in Mesozoic South China: a flat-slab subduction model. Geology 35 (2), 179–182.
Li, X.H., Chen, Z.G., Liu, D.Y., Li, W.X., 2003. Jurassic gabbro–granite–syenite suites from Southern Jiangxi Province, SE China: age, origin, and tectonic significance. International Geology Review 45 (10), 898–921.
Li, X.H., Chen, S.D., Luo, J.H., Wang, Y., Cao, K., Liu, L., 2011. LA–ICP–MS U–Pb Isotope chronology of the single zircons from Early Cretaceous Jiande Group in Western Zhejiang, SE China: significances to stratigraphy. Geological Review 57 (6), 825–836 (in Chinese).
Li, X.H., Chung, S.L., Zhou, H.W., Lo, C.H., Liu, Y., Chen, C.H., 2004. Jurassic intraplate magmatism in southern Hunan–eastern Guangxi: ^{40}Ar/^{39}Ar dating, geochemistry, Sr–Nd isotopes and implications for the tectonic evolution of SE China. Geological Society, London, Special Publications 226 (1), 193–215.
Li, X.H., Hu, R.Z., Rao, B., 1997. Geochronology and geochemistry of Cretaceous mafic dikes from northern Guangdong, SE China. Geochemica 26 (2), 14–31 (in Chinese).
Li, X.H., Li, W.X., Li, Z.X., 2007. On the genetic classification and tectonic implications of the Early Yanshanian granitoids in the Nanling Range, South China. Chinese Science Bulletin 52 (14), 1873–1885.
Li, W.X., Li, X.H., Li, Z.X., Lou, F.S., 2008. Obduction-type granites within the NE Jiangxi Ophiolite: implications for the final amalgamation between the Yangtze and Cathaysia Blocks. Gondwana Research 13, 288–301.
Li, Z.X., Li, X.h., Zhou, H., Kinny, P.D., 2002. Grenvillian continental collision in south China: new SHRIMP U–Pb zircon results and implications for the configuration of Rodinia. Geology 30 (2), 163–166.
Li, Z.L., Zhou, J., Mao, J.R., Santosh, M., Yu, M.G., Li, Y.Q., Hu, Y.Z., Langmuir, C.H., Chen, Z.X., Cai, X.X., Hu, Y.H., 2013. Zircon U–Pb geochronology and geochemistry of two episodes of granitoids from the northwestern Zhejiang Province, SE China: implication for magmatic evolution and tectonic transition. Lithos 179 (0), 334–352.

Li, X.H., Zhou, G., Zhao, J., Fanning, C.M., Compston, W., 1994. SHRIMP ion microprobe zircon U–Pb age of the NE Jiangxi ophiolite and its tectonic implications. Chinese Journal of Geochemistry 13 (4), 317–325.

Li, X.H., et al., 2009. Amalgamation between the Yangtze and Cathaysia Blocks in South China: constraints from SHRIMP U–Pb zircon ages, geochemistry and Nd–Hf isotopes of the Shuangxiwu volcanic rocks. Precambrian Research 174 (1–2), 117–128.

Liao, Q.A., Li, C.N., Wang, J.M., 1999. Characteristics and geological significance of S-type acid volcanic rocks in Late Jurassic along Jiangshao rift zone. Earth Science—Journal of China University of Geoscience 24 (1), 63–68 (in Chinese).

Liu, X., Fan, H.R., Santosh, M., Hu, F.F., Yang, K.F., Li, Q.L., Yang, Y.H., Liu, Y.S., 2012. Remelting of Neoproterozoic relict volcanic arcs in the Middle Jurassic: implication for the formation of the Dexing porphyry copper deposit. Southeastern China. Lithos **150**, 85–100.

Liu, Y.S., Gao, S., Hu, Z.C., Gao, C.G., Zong, K.Q., Wang, D.B., 2010a. Continental and oceanic crust recycling-induced melt–peridotite interactions in the trans-north China orogen: U–Pb dating, Hf isotopes and trace elements in zircons from mantle xenoliths. Journal of Petrology 51 (1–2), 537–571.

Liu, S., Hu, R.Z., Gao, S., Feng, C.X., Qi, Y.Q., Wang, T., Feng, G.Y., Coulson, I.M., 2008a. U–Pb zircon age, geochemical and Sr–Nd–Pb–Hf isotopic constraints on age and origin of alkaline intrusions and associated mafic dikes from Sulu orogenic belt, Eastern China. Lithos 106 (3-4), 365–379.

Liu, S., Hu, R.Z., Gao, S., Feng, C.X., Qi, L., Zhong, H., Xiao, T.F., Qi, Y.Q., Wang, T., Coulson, I.M., 2008b. Zircon U–Pb geochronology and major, trace elemental and Sr–Nd–Pb isotopic geochemistry of mafic dykes in western Shandong Province, east China: constrains on their petrogenesis and geodynamic significance. Chemical Geology 255 (3–4), 329–345.

Liu, S., Hu, R., Gao, S., Feng, C., Yu, B., Feng, G., Qi, Y., Wang, T., Coulson, I.M., 2009. Petrogenesis of Late Mesozoic mafic dykes in the Jiaodong Peninsula, eastern North China Craton and implications for the foundering of lower crust. Lithos 113 (3–4), 621–639.

Liu, Y.S., Hu, Z.C., Gao, S., Günther, D., Xu, J., Gao, C.G., Chen, H.H., 2008c. In situ analysis of major and trace elements of anhydrous minerals by LA–ICP–MS without applying an internal standard. Chemical Geology 257 (1–2), 34–43.

Liu, Y.S., Hu, Z.C., Zong, K.Q., Gao, C.G., Gao, S., Xu, J., Chen, H.H., 2010b. Reappraisement and refinement of zircon U–Pb isotope and trace element analyses by LA–ICP–MS. Chinese Science Bulletin 55 (15), 1535–1546.

Ludwig, K.R., 2003. ISOPLOT 3.00: a geochronological toolkit for Microsoft Excel. Berkeley Geochronology Center, California, Berkeley (39 pp.).

Mao, J.R., Chen, R., Li, J.Y., Ye, H.M., Zhao, X.L., 2006. Geochronology and geochemical characteristics of late Mesozoic granitic rocks from southwestern Fujian and their tectonic evolution. Acta Petrologica Sinica 22 (6), 1723–1734 (in Chinese).

Mao, J.W., Xie, G.Q., Guo, C.L., Chen, Y.C., 2007. Large-scale tungsten-tin mineralization in the South China: metallogenic ages and corresponding geodynamic process. Acta Petrologica Sinica 23 (10), 2329–2338 (in Chinese).

Mao, J.W., Xie, G.Q., Guo, C.L., Yuan, S.D., Cheng, Y.B., Chen, Y.C., 2008. Spatial-temporal distribution of Mesozoic ore deposits in South China and their metallogenic settings. Geological Journal of China University 14 (4), 510–526 (in Chinese).

Mao, J.W., Xie, G.Q., Li, X.F., Zhang, C.Q., Mei, Y.X., 2004. Mesozoic large scale mineralization and multiple lithospheric extension in South China. Earth Science Frontiers 11 (1), 45–55 (in Chinese).

Maruyama, S., Send, T., 1986. Orogeny and relative plate motions: example of the Japanese Islands. Tectonophysics 127 (3–4), 305–329.

Münker, C., Pfänder, J.A., Weyer, S., Büchl, A., Kleine, T., Mezger, K., 2003. Evolution of planetary cores and the earth–moon system from Nb/Ta systematics. Science 301 (5629), 84–87.

Niu, Y., O'Hara, M.J., 2009. MORB mantle hosts the missing Eu (Sr, Nb, Ta and Ti) in the continental crust: new perspectives on crustal growth, crust–mantle differentiation and chemical structure of oceanic upper mantle. Lithos 112 (1–2), 1–17.

O'Reilly, S.Y., Zhang, M., 1995. Geochemical characteristics of lava-field basalts from eastern Australia and inferred sources: connections with the subcontinental lithospheric mantle? Contributions to Mineralogy and Petrology 121 (2), 148–170.

Pertermann, M., Hirschmann, M.M., 2003. Partial melting experiments on a MORB-like pyroxenite between 2 and 3 GPa; constraints on the presence of pyroxenite in basalt source regions from solidus location and melting rate. Journal of Geophysical Research B108 (2125).

Pfänder, J.A., Münker, C., Stracke, A., Mezger, K., 2007. Nb/Ta and Zr/Hf in ocean island basalts—implications for crust-mantle differentiation and the fate of Niobium. Earth and Planetary Science Letters 254 (1–2), 158–172.

Qi, L., Hu, J., Gregoire, D.C., 2000. Determination of trace elements in granites by inductively coupled plasma mass spectrometry. Talanta 51 (3), 507–513.

Qi, Y.Q., Hu, R.Z., Liu, S., Coulson, I.M., Qi, H.W., Tian, J.J., Feng, C.X., Wang, T., 2012. Geochemical and Sr–Nd–Pb isotopic compositions of Mesozoic mafic dikes from the Gan–Hang tectonic belt, South China: petrogenesis and geodynamic significance. International Geology Review 54 (8), 920–939.

Rapp, R.P., Shimizu, N., Norman, M.D., 2003. Growth of early continental crust by partial melting of eclogite. Nature 425, 605–609.

Rapp, R.P., Shimizu, N., Norman, M.D., Applegate, G.S., 1999. Reaction between slabderived melts and peridotite in the mantle wedge: experimental constraints at 3.8 GPa. Chemical Geology 160, 335–356.

Rapp, R.P., Watson, E.B., Miller, C.F., 1991. Partial melting of amphibolite/eclogite and theorigin of Archean trondhjemites and tonalites. Precambrian Research 51, 1–25.

Ratschbacher, L., Hacker, B.R., Webb, L.E., McWilliams, M., Ireland, T., Dong, S.W., Calvert, A., Chateigner, D., Wenk, H.R., 2000. Exhumation of the ultrahigh-pressure continental crust in east central China: Cretaceous and Cenozoic unroofing and the Tan–Lu fault. Journal of Geophysical Research 105 (B6), 13303–13338.

Rudnick, R.L., Fountain, D.M., 1995. Nature and composition of the continental crust: a lower crustal perspective. Reviews in Geophysics 33 (3), 267–309.

Rudnick, R.L., Gao, S., 2003. Composition of the continental crust. Treatise on geochemistry 3, 1–64.

Rudnick, R.L., Barth, M., Horn, I., McDonough, W.F., 2000. Rutile-bearing refractory eclogites: missing link between continents and depleted mantle. Science 287 (5451), 278–281.

Sobolev, A.V., Hofmann, A.W., Kuzmin, D.V., Yaxley, G.M., Arndt, N.T., Chung, S.-L., Danyushevsky, L.V., Elliott, T., Frey, F.A., Garcia, M.O., Gurenko, A.A., Kamenetsky, V.S., Kerr, A.C., Krivolutskaya, N.A., Matvienkov, V.V., Nikogosian, I.K., Rocholl, A., Sigurdsson, I.A., Sushchevskaya, N.M., Tekley, M., 2007. The amount of recycled crust in sources of mantle-derived melts. Science 316, 412–417.

Sun, S.S., McDonough, W.F., 1989. Chemical and isotopic systematics of oceanic basalts: implications for mantle composition and processes. Geological Society, London, Special Publications **42** (1), 313–345.

Takahashi, E., Kushiro, I., 1983. Melting of a dry peridotite at high pressures and basalt magma genesis. American Mineralogist 68, 859–879.

Tiepolo, M., Vannucci, R., Oberti, R., Foley, S., Bottazzi, P., Zanetti, A., 2000. Nb and Ta incorporation and fractionation in titanian pargasite and kaersutite: crystal-chemical constraints and implications for natural systems. Earth and Planetary Science Letters 176 (2), 185–201.

Tong, W.X., Tobisch, O.T., 1996. Deformation of granitoid plutons in the Dongshan area, southeast China: constraints on the physical conditions and timing of movement along the Changle–Nanao shear zone. Tectonophysics 267 (1–4), 303–316.

Walter, M.J., 1998. Melting of garnet peridotite and the origin of komatiite and depleted lithosphere. Journal of Petrology 39 (1), 29–60.

Wang, D.Z., 2004. The study of granitic rocks in South China: looking back and forward. Geological Journal of China Universities 10 (3), 305–314 (in Chinese).

Wang, Y.J., Fan, W.M., Guo, F., Peng, T.P., Li, C.W., 2003. Geochemistry of Mesozoic mafic rocks adjacent to the Chenzhou–Linwu fault, South China: implications for the lithospheric boundary between the Yangtze and Cathaysia blocks. International Geology Review 45 (3), 263–286.

Wang, Y.J., Fan, W.M., Peng, T.P., Guo, F., 2005. Elemental and Sr–Nd isotopic systematics of the early Mesozoic volcanic sequence in southern Jiangxi Province, South China: petrogenesis and tectonic implications. International Journal of Earth Sciences 94 (1), 53–65.

Wang, Y.J., Fan, W.M., Zhang, G.W., Zhang, Y.H., 2013a. Phanerozoic tectonics of the South China Block: key observations and controversies. Gondwana Research 23 (4), 1273–1305.

Wang, Y., Guan, T.Y., Huang, G.F., Yu, D.G., Chen, C.L., 2002. Isotope chronological studies of late Yanshanian volcanic rocks in northeast Jiangxi Province. Acta Geoscientia Sinica 23 (3), 233–236 (in Chinese).

Wang, Z.Q., Li, Z.Y., Tang, J.W., 2013b. Deep geodynamic mechanism of the volcanic-type uranium mineralization in Xinlu Basin, western Zhejiang province. Acta Geoscientia Sinica 87 (5), 703–714 (in Chinese).

Wang, Y.J., Liao, C.L., Fan, W.M., Peng, T.P., 2004a. Early Mesozoic OIB-type alkaline basalt in central Jiangxi Province and its tectonic implications. Geochimica 33 (2), 109–117 (in Chinese).

Wang, Q., Wyman, D.A., Xu, J.F., Zhao, Z.H., Jian, P., Zi, F., 2007. Partial melting of thickened or delaminated lower crust in the middle of Eastern China: implications for Cu-Au mineralization. The Journal of Geology 115 (2), 149–163.

Wang, Q., Xu, J.F., Jian, P., Bao, Z.W., Zhao, Z.H., Li, C.F., Xiong, X.L., Ma, J.L., 2006. Petrogenesis of adakitic porphyries in an extensional tectonic setting, Dexing, South China: implications for the genesis of porphyry copper mineralization. Journal of Petrology 47 (1), 119–144.

Wang, Q., Zhao, Z.H., Jian, P., Xu, J.F., Bao, Z.W., Ma, J.L., 2004b. SHRIMP zircon geochronology and Nd-Sr isotopic geochemistry of the Dexing granodiorite porphyries. Acta Petrologica Sinica 20 (2), 315–324 (in Chinese).

Wu, F.Y., Ce, W.C., Sun, D.Y., Guo, C.L., 2003. Discussion on the lithospheric thinning in eastern China. Earth Science Frontiers 10 (3), 51–60 (in Chinese).

Xie, G.Q., 2003. Late Mesozoic and Cenozoic Mafic Dikes (bodies) from Southeastern China: geological and geochemical characteristics and its geodynamics–a case of Jiangxi Province. Guiyang, Institute of Geochemistry, Chinese Academy of Science 1–126 (in Chinese).

Xie, G.Q., Mao, J.W., Hu, R.Z., Li, R.L., Cao, J.J., 2005b. Geological and geochemical characteristics of early Tertiary basaltic rocks in center Jiangxi province, Southeast China and their geological implication. Acta Petrologica Sinica 21 (1), 77–90 (in Chinese).

Xie, G.Q., Mao, J.W., Hu, R.Z., Li, R.L., Jiang, G.H., Cao, J.J., Zhao, J.H., 2005a. Jurassic intra-plate basaltic magmatism in Southeast China: evidence from geological and geochemical characteristics of the Chebu Gabbroite in Southern Jiangxi Province. Acta Geologica Sinica 79 (5), 662–672.

Xu, X.S., 2008. Several problems worthy to be noticed in the research of granites and volcanic rocks in SE China. Geological Journal of China Universities 14 (3), 283–294 (in Chinese).

Xu, Y.G., 2014. Recycled oceanic crust in the source of 90–40 Ma basalts in North and Northeast China: evidence, provenance and significance. Geochimica et Cosmochimica Acta 143, 49–67.

Xu, X.S., Xie, X., 2005. Late Mesozoic-Cenozoic basaltic rocks and crust-mantle interaction, SE China. Geological Journal of China Universities 14 (3), 283–294 (in Chinese).

Xu, X.S., O'Reilly, S.Y., Griffin, W.L., Zhou, X.M., 2000. Genesis of Young lithospheric mantle in southeastern China: an LAM–ICPMS trace element study. Journal of Petrology 41 (1), 111–148.

Xu, Y.G., Ross, J.V., Mercier, J.C.C., 1993. The upper mantle beneath the continental rift of Tanlu, Eastern China: evidence for the intra-lithospheric shear zones. Tectonophysics 225 (4), 337–360.

Xu, Y.G., Sun, M., Yan, W., Liu, Y., Huang, X.L., Chen, X.M., 2002. Xenolith evidence for polybaric melting and stratification of the upper mantle beneath South China. Journal of Asian Earth Sciences 20 (8), 937–954.

Yan, J., Chen, J.F., 2007. Geochemistry of Qingshan formation colcanic rocks from Jiaolai basin, eastern Shandong province: petrogenesis and geological significance. Geochimica 36 (1), 1–10 (in Chinese).
Yang, S.Y., Jiang, S.Y., Jiang, Y.H., Zhao, K.D., Fan, H.H., 2010. Zircon U–Pb geochronology, Hf isotopic composition and geological implications of the rhyodacite and rhyodacitic porphyry in the Xiangshan uranium ore field, Jiangxi Province, China. Science China Earth Sciences 53 (10), 1411–1426.
Yang, S.Y., Jiang, S.Y., Zhao, K.D., Jiang, Y.H., Ling, H.F., Luo, L., 2012. Geochronology, geochemistry and tectonic significance of two Early Cretaceous A-type granites in the Gan–Hang Belt, Southeast China. Lithos 150 (0), 155–170.
Yaxley, G.M., 2000. Experimental study of the phase and melting relations of homogeneous basalt + peridotite mixtures and implications for the petrogenesis of flood basalts. Contributions to Mineralogy and Petrology 139, 326–338.
Yu, Y.W., Jiang, Y., Lu, C.Z., 2008. Stratigraphic subdivision and neodymium isotope characteristics of the Cretaceous volcanic rocks in Zhejiang province. Journal of Stratigraphy 32 (1), 69–78 (in Chinese).
Yu, X.Q., Shu, L.S., Yan, T.Z., Yu, Y.W., Zu, F.P., Wang, B., 2004. Geochemistry of basalts of late period of Early Cretaceous from Jiangshan–Guangfeng, SE China and its tectonic significance. Geochimica 33 (5), 465–476 (in Chinese).
Yu, X.Q., Wu, G.G., Shu, L.S., Yan, T.Z., Zhang, D., Di, Y.J., 2006. The Cretaceous tectonism of the Gan–Han Tectonic Belt, southeastern China. Earth Science Frontiers 13 (3), 31–43 (in Chinese).
Yui, T.F., Heaman, L., Lan, C.Y., 1996. U–Pb and Sr isotopic studies on granitoids from Taiwan and Chinmen–Lieyü and tectonic implications. Tectonophysics 263 (1–4), 61–76.
Zhang, X.F., 1999. Formation and evolution of Mesozoic volcanic basin in Gan–Hang Tectonic Belt. Uranium Geology 15 (1), 18–23 (in Chinese).
Zhang, G.W., Guo, A.L., Wang, Y.J., Li, S.Z., Dong, Y.P., Liu, S.F., He, D.F., Cheng, S.Y., Lu, R.K., Yao, A.P., 2013. Tectonics of South China continent and its implications. Science China Earth Sciences 56 (11), 1804–1828.
Zhang, J.J., Zheng, Y.F., Zhao, Z.F., 2009. Geochemical evidence for interaction between oceanic crust and lithospheric mantle in the origin of Cenozoic continental basalts in east-central China. Lithos 110, 305–326.
Zhao, J.H., 2004. Chronology and geochemistry of mfic rocks from Fujian Province: implications for the mantle evolution of SE China since Late Mesozoic. Guiyang, Institute of Geochemistry, Chinese Academy of Science 1–107 (in Chinese).
Zhao, Z.H., Bao, Z.W., Zhang, B.Y., 1998. Geochemistry of the Mesozoic basaltic rocks in southern Hunan Province. Science in China, Ser. D 41, 102–112 (Supp.).
Zhao, Z.F., L.Q, D., Zheng, Y.F., 2015. Two types of the crust–mantle interaction in continental subduction zones. Science China: Earth Sciences 58, 1269–1283.
Zhao, J.H., Zhou, M.F., Yan, D.P., Zheng, J.P., Li, J.W., 2011. Reappraisal of the ages of Neoproterozoic strata in South China: no connection with the Grenvillian orogeny. Geology 39 (4), 299–302.
Zheng, Y.F., 2012. Metamorphic chemical geodynamics in continental subduction zones. Chemical Geology 328 (0), 5–48.
Zhou, J.Z., 2000. Characteristics of Mesozoic magmatic rocks in western Zhejiang and their relation with uranium mineralization. Uranium Geology 16 (3), 143–149 (in Chinese).
Zhou, X.M., 2003. My thinking about granite geneses of South China. Geological Journal of China Universities 9 (4), 556–565 (in Chinese).
Zhou, J.C., Chen, R., 2001. Geochemistry of late Mesozoic interaction between crust and mantle in southeastern Fujian Province. Geochimica 30 (6), 547–558 (in Chinese).
Zhou, X.M., Li, W.X., 2000. Origin of Late Mesozoic igneous rocks in Southeastern China: implications for lithosphere subduction and underplating of mafic magmas. Tectonophysics 326 (3–4), 269–287.
Zhu, W.G., Zhong, H., Li, X.H., He, D.F., Song, X.Y., Ren, T., Chen, Z.Q., Sun, H.S., Liao, J.Q., 2010. The early Jurassic mafic–ultramafic intrusion and A-type granite from northeastern Guangdong, SE China: age, origin, and tectonic significance. Lithos 119 (3–4), 313–329.